ON MACHINE-LEARNED CLASSIFICATION OF VARIABLE STARS WITH SPARSE AND NOISY TIME-SERIES DATA

JOSEPH W. RICHARDS[1,2,*], DAN L. STARR[1], NATHANIEL R. BUTLER[1], JOSHUA S. BLOOM[1], JOHN M. BREWER[3], ARIEN CRELLIN-QUICK[1], JUSTIN HIGGINS[1], RACHEL KENNEDY[1], MAXIME RISCHARD[1]

Draft version October 22, 2018

ABSTRACT

With the coming data deluge from synoptic surveys, there is a growing need for frameworks that can quickly and automatically produce calibrated classification probabilities for newly-observed variables based on a small number of time-series measurements. In this paper, we introduce a methodology for variable-star classification, drawing from modern machine-learning techniques. We describe how to homogenize the information gleaned from light curves by selection and computation of real-numbered metrics (features), detail methods to robustly estimate periodic light-curve features, introduce tree-ensemble methods for accurate variable star classification, and show how to rigorously evaluate the classification results using cross validation. On a 25-class data set of 1542 well-studied variable stars, we achieve a 22.8% overall classification error using the random forest classifier; this represents a 24% improvement over the best previous classifier on these data. This methodology is effective for identifying samples of specific science classes: for pulsational variables used in Milky Way tomography we obtain a discovery efficiency of 98.2% and for eclipsing systems we find an efficiency of 99.1%, both at 95% purity. We show that the random forest (RF) classifier is superior to other machine-learned methods in terms of accuracy, speed, and relative immunity to features with no useful class information; the RF classifier can also be used to estimate the importance of each feature in classification. Additionally, we present the first astronomical use of hierarchical classification methods to incorporate a known class taxonomy in the classifier, which further reduces the catastrophic error rate to 7.8%. Excluding low-amplitude sources, our overall error rate improves to 14%, with a catastrophic error rate of 3.5%.

Subject headings: stars: variables: general – methods: data analysis – methods: statistical – techniques: photometric

[1] Astronomy Department, University of California, Berkeley, CA, 94720-7450, USA
[2] Statistics Department, University of California, Berkeley, CA, 94720-7450, USA
[3] Astronomy Department, Yale University, New Haven, CT 06520-8101, USA
[*] E-mail: jwrichar@stat.berkeley.edu

1. INTRODUCTION

Variable star science (e.g., Eyer & Mowlavi 2008) remains at the core of many of the central pursuits in astrophysics: *pulsational* sources probe stellar structure and stellar evolution theory, *eruptive and episodic* systems inform our understanding of accretion, stellar birth, and mass loss, and *eclipsing* systems constrain mass transfer, binary evolution, exoplanet demographics, and the mass-radius-temperature relation of stars. Some eclipsing systems and many of the most common pulsational systems (e.g., RR Lyrae, Cepheids, and Mira variables) are the fundamental means to determine precise distances to clusters, to relic streams of disrupted satellites around the Milky Way, and to the local group of galaxies. They anchor the measurement of the size scale of the Universe. See Walkowicz et al. (2009) for a recent review.

The promise of modern synoptic surveys (Ivezić et al. 2007), such as the Large Synoptic Survey Telescope (LSST), is the promise of discovery of many new instances of variable stars (Sesar et al. 2007), some to be later studied individually with greater photometric and spectroscopic scrutiny[5] and some to be used as ensemble probes to larger volumes. New classes (with variability reflecting physics not previously seen) and rare instances of existing classes of variables are almost certainly on the horizon (e.g., Covey et al. 2007).

Classification of variable stars—the identification of a certain variable with a previously identified group ("class") of sources presumably of the same physical origin—presents several challenges. First, time-series data alone (i.e., without spectroscopy) provides an incomplete picture of a given source: this picture is even less clear the more poorly sampled the light curve is both in time and in precision. Second, on conceptual grounds, the observation of variability does not directly reveal the underlying physical mechanisms responsible for the variability. What the totality of the characteristics *are* that define the nature of the variability may in principle be known at the statistical level. But *why* that variability is manifest relies on an imperfect mapping of an inherently incomplete physical model to the data. (For example, the periodic dimming of a light curve may be captured with a small number of observable parameters but the inference that that source is an eclipsing one requires a theoretical framework.) This intermingling of observation and theory has given rise to a taxonomy of variable stars (for instance, defined in the GCVS[6]) that is based on an admixture of phenomenology and physics. Last, on logistical grounds, the data volume of time-series surveys may be too large for human-intensive analysis, follow-up, and classification (which benefits from domain-specific knowledge and insight).

While the data deluge problem suggests an obvious role for computers in classification[7], the other challenges also naturally lend themselves to algorithmic and computational solutions. Individual light curves can be automatically analyzed with a variety of statistical tools and the outcome of those analyses can be handled with machine-learning algorithms that work with existing taxonomies (however fuzzy the boundary between classes) to produce statistical statements about the source classification. Ultimately, with a finite amount of time-series data we wish to have well-calibrated probabilistic statements about the physical origin and phenomenological class of that source.

While straightforward in principle, providing a machine-learned classifier that is accurate, fast, and well-calibrated is an extraordinarily difficult task on many fronts (see discussion in Eyer et al. 2008). There may be only a few instances of light curves in a given class ("labelled data") making training and validation difficult. Even with many labelled instances, in the face of noisy, sometimes spurious, and sparsely sampled data, there is a limit to the statistical inferences that can be gleaned from a single light curve. Some metrics (called, in machine-learning parlance, "features") on the light curve may be very sensitive to the signal-to-noise of the data and others, particularly frequency-domain features, may be sensitive to the precise cadences of the survey (§4.9). For computationally intensive feature generation (e.g., period searches) fast algorithms may be preferred over slower but more robust algorithms.

Machine learning in variable star classification has been applied to several large time-series datasets (Woźniak et al. 2004; Willemsen & Eyer 2007; Debosscher et al. 2007; Mahabal et al. 2008; Sarro et al. 2009; Blomme et al. 2010). A common thread for most previous work is application of a certain machine-learning framework to a single survey. And, most often, the classification is used to distinguish/identify a small set of classes of variables (e.g., Miras and other red giant variability). Debosscher et al. (2007) was the first work to tackle the many-class (> 20) problem with multiple survey streams. Debosscher et al. (2007) also explored several classification frameworks and quantitatively compared the results.

The purpose of this work is to build a many-class classification framework by exploring in detail each aspect of the classification of variable stars: proper feature creation and selection in the presence of noise and spurious data (§2), fast and accurate classification (§3), and improving classification by making use of the taxonomy. We present a formalism for evaluating the results of the classification in the context of expected statistical risk for classifying new data. We use data analyzed by Debosscher et al. to allow us to make direct comparison with those results (§4). Overall, we find a 24% improvement in the misclassification rate with the same data. The present work only makes use of metrics derivable from time-domain observations in a single bandpass; color information and context (i.e., the location of the variable in the Galaxy and with respect to other catalog sources) are not used. In future work, we will explore how machine-learned classifiers can be applied across surveys (with different characteristics) and how context and time-domain features can be used in tandem to improve overall classification.

---

[5] High-precision photometry missions (Kepler, MOST, CoRoT, etc.) are already challenging the theoretical understanding of the origin of variability and the connection of some specific sources to established classes of variables.

[6] General Catalog of Variable Stars, http://www.sai.msu.su/groups/cluster/gcvs/gcvs/

[7] Not discussed herein are the challenges associated with *discovery* of variability. See Shin et al. (2009) for a review.

2. HOMOGENIZING LIGHT CURVES: FEATURE GENERATION

Classification fundamentally relies upon the ability to recognize and quantify the differences between light curves. To build a classifier, many *instances* of light curves are required for each class of interest. These labelled instances are used in the *training* and *testing* process (§3). Since the data are not, in general, sampled at regular intervals nor are all instances of a certain class observed with the same number of epochs and signal-to-noise, identifying the differences directly from the time-series data is exceedingly challenging both conceptually and computationally (cf. Eads et al. 2004). Instead we homogenize the data by transforming each light curve into a set of real-number line features using statistical and model-specific fitting procedures. For variable stars, features fall into two broad categories: those related to the period of the source (and harmonics) and those that are not. Which features to use (and not use) is an important question that we will address herein. We also address the effects of (implicit) correlation of certain features in affecting the classification model.

Appendix A provides an account of the non-periodic features used in this present work; many of these are simple statistics on the distribution of the fluxes (e.g., median absolute deviation and min-max amplitude) and some are domain specific (such as a feature that captures how much a source varies like the damped random walk seen in quasars; Butler & Bloom 2010). Since the period and periodic signatures of a variable are such crucial quantitative measurements, yet tend to be difficult to infer from simple prescriptions, we review the algorithms we employ to compute these features.

2.1. *Robust estimation of periodic features*

2.1.1. *A Fast Period Search Including Measurement Uncertainty*

We model the photometric magnitudes of variable stars versus time t as a superposition of sines and cosines, starting from the most basic form:

$$y_i(t|f_i) = a_i \sin(2\pi f_i t) + b_i \cos(2\pi f_i t) + b_{i,\circ}, \tag{1}$$

where a and b are normalization constants for the sinuoids of frequency f_i, and $b_{i,\circ}$ is the magnitude offset. For each variable star, we record at each epoch, t_k, a photometric magnitude, d_k, and its uncertainty, σ_k. To search for periodic variations in these data, we fit (1) by minimizing the sum of squares

$$\chi^2 = \sum_k [d_k - y_i(t_k)]^2/\sigma_k^2, \tag{2}$$

where σ_k is the measurement uncertainty in data point d_k. As discussed in Zechmeister & Kürster (2009), this least-squares fitting of sinusoids with a floating mean and over a range of test frequencies is closely similar to an evaluation of the well-known Lomb-Scargle (Lomb 1976; Barning 1963; Scargle 1982) periodogram. Allowing the mean to float leads to more robust period estimates in the cases where the periodic phase is not uniformly sampled; in these cases, the model light curve has a non-zero mean. (This is particularly important for searching for periods on timescales similar to the data span $T_{\rm tot}$.) If we define:

$$\chi_\circ^2 = \sum_k [d_k - \mu]^2/\sigma_k^2, \tag{3}$$

with the weighted mean $\mu = \sum_k [d_k/\sigma_k^2] / \sum_k 1/\sigma_k^2$, then our generalized Lomb-Scargle periodogram P_f is

$$P_f(f) = \frac{(N-1)}{2} \frac{\chi_\circ^2 - \chi_m^2(f)}{\chi_\circ^2}, \tag{4}$$

where $\chi_m^2(f)$ is χ^2 minimized with respect to a, b, and $b_\circ$. For the NULL hypothesis of no periodic variation and a white noise spectrum, we expect P_f to be F-distributed with 2 numerator and $N-1$ denominator degrees of freedom. A similar periodogram statistic and NULL distribution is derived in Gregory (2005) by marginalizing over an unknown scale error in the estimation of the uncertainties. In the limit of many data, the NULL distribution takes the well-known exponential form (e.g., Zechmeister & Kürster 2009). For all $\sigma_i = 1$, (4) becomes the standard Lomb-Scargle periodogram. In addition to the benefits of allowing a floating mean, the generalized Lomb-Scargle periodogram (4) has two principal advantages over the standard formula: (1) uncertainties on the measurements are included, and because $P_f(f)$ is a constructed from a ratio of two sums-of-squares, (2) there can be scale errors on the determination of these uncertainties (c.f., Gregory 2005).

We undertake the search for periodicity in each source by evaluating (4) on a linear test grid in frequency from a minimum value of $1/T_{\rm tot}$ to a maximum value of 20 cycles per day, in steps of $\delta f = 0.1/T_{\rm tot}$. This follows closely the prescription in Debosscher et al. (2007), with the important exception that we search for periods up to 20 cycles per day in all sources, whereas Debosscher et al. (2007) search up to a "pseudo" Nyquist frequency ($f_N = 0.5\langle 1/\Delta T\rangle$, where ΔT is the difference in time between observations and $\langle \cdot \rangle$ is an average) for most sources but allow the maximum frequency value to increase for certain source classes. To avoid favoring spurious high-frequency peaks in the periodogram, we subtract a mild penalty of $\log f/f_N$ above f_N from $P_f(f)$ above $f = f_N$. Significance of the highest peak is the evaluated from $P_f(f)$. We apply an approximate correction for the number of search trials using the prescription of Horne & Baliunas (1986), although we note that numerical simulations suggest these significance estimates underestimate the number of true trials and are uniformly high by 1–2σ.
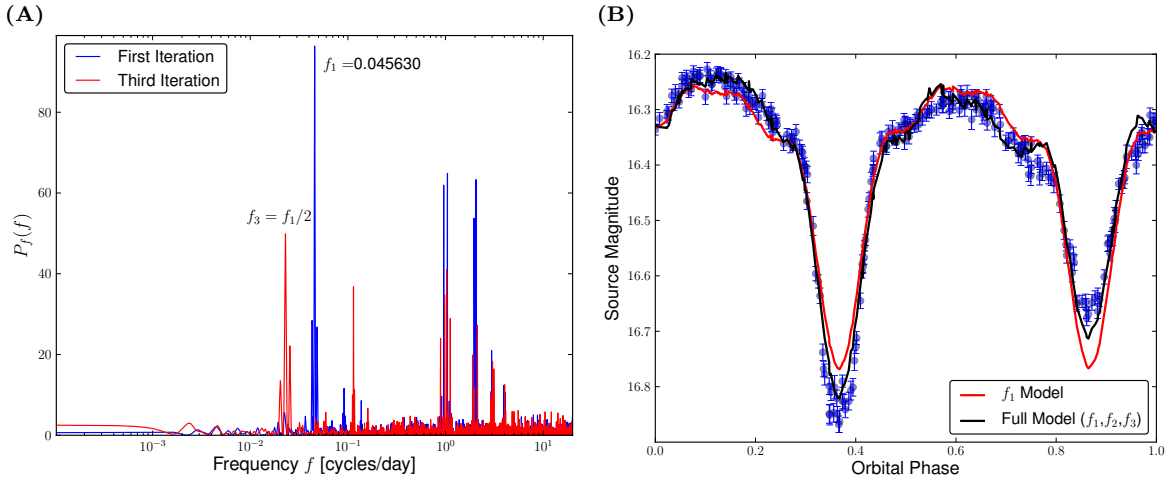
(A) **(B)**

FIG. 1.— (A) Generalized Lomb-Scargle Periodogram $P_f(f)$ for an eclipsing source in the sample. Plotted in blue is the first iteration to find peak frequency f_1, which is twice the orbital frequency f_3 (third iteration plotted in red). In this case, the second iteration yielded $f_2 = 3f_3$. For eclipsing sources, our $P_f(f)$ analysis which utilizes a sine and cosine fit without harmonics, tends to place the orbital period in either f_2 or f_3. (B) The light curve folded at the orbital period f_3. Over plotted is the best-fit model considering only f_1 (plus 3 harmonics; in red), which fails to account for the difference in primary and secondary eclipse depths. Addition of the 2nd and 3rd frequency component models (black curve) account for the full light curve structure well.

Standard "fast" implementations of the Lomb-Scargle periodogram (e.g., Press et al. 2001), which scale with the number of frequency bins N_f as $N_f \log N_f$, are not particularly fast for our purposes. This is because we wish to sample relatively few data ($N \sim 100$) on a very dense, logarithmic frequency grid $N_f \sim 10^6$. It is more fruitful to pursue algorithms which scale with N. We find that standard implementations are sped up by a factor of ~ 10 by simply taking care in calculating the sines and cosines that are necessary to tabulate (4). Instead of calculating all the sines and cosines at a given time point at each of the N_f frequency bins, we calculate sine and cosine only once at $f = \delta f$ and then use trigonometric identities (i.e., successive rotations by an angle $2\pi\delta f t_i$) to determine the sines and cosines at higher frequencies.

2.1.2. *Fitting Multiple Periods*

Following Debosscher et al. (2007), we fit each light curve with a linear term plus a harmonic sum of sinusoids:

$$y(t) = ct + \sum_{i=1}^{3}\sum_{j=1}^{4} y_i(t|jf_i), \tag{5}$$

where each of 3 test frequencies f_i are allowed to have 4 harmonics at frequencies $f_{i,j} = jf_i$. The 3 test frequencies f_i are found iteratively, by successively finding the periodogram peaks in $P_f(f)$. This procedure assumes a model with no harmonics, only the fundamental. We then relax this assumption by fitting for the fundamental plus 3 harmonics of the fundamental. Unlike Debosscher et al. (2007) who fit for the linear term prior to fitting sines and cosines, we evaluate the best-fit linear term at each test frequency during the search for the first periodogram peak, using a modification of (4) to fit for the linear trend coefficient c at the same time as the constants a_0, b_0, and $b_{0,\circ}$. The value for c is updated when we then calculate the 4-harmonic fit (plus linear term) around the first best-fit frequency. The quantity $\chi_\circ^2$ is updated after the ith iteration and subtraction of each 4-harmonic component is performed prior to calculating $P_f(f)$.

In reporting the values from the fit of (5), we ignore the constant offsets $b_{i,\circ}$. We translate the sinusoid coefficients into an amplitude and a phase:

$$A_{i,j} = \sqrt{a_{i,j}^2 + b_{i,j}^2} \tag{6}$$

$$PH_{i,j} = \tan^{-1}(b_{i,j}, a_{i,j}). \tag{7}$$

Here $A_{i,j}$ ($PH_{i,j}$) is the amplitude (phase) of the jth harmonic of the ith frequency component. Following Debosscher et al. (2007), we correct the phases $PH_{i,j}$ to relative phases with respect to the phase of the first component $PH'_{i,j} = PH_{i,j} - PH_{00}$. This is to preserve comparative utility in the phases for multiple sources by dropping a non-informative phase offset for each source. All phases are then remapped to the interval $|-\pi, +\pi|$.

A list and summary of all of the period features used in our analysis is found in table 4 in Appendix A.

2.2. *Non-periodic light curve features*

In seeking to classify variable star light curves, it may not always be possible to characterize flux variation purely by detecting and characterizing periodicity. We find that simple summary statistics of the flux measurements (e.g., standard deviation, skewness, etc.) — determined without sorting the data in time or period phase — give a great deal of predictive power. For instance, skewness is very effective for separating eclipsing from non-eclipsing sources. We define (in Appendix A) 20 non-periodic features and explore in §4 their utility for source classification. A summary of all of the non-period features used in our analysis is found in table 5 in Appendix A.

When only a small number of epochs ($\lesssim 12$) are sampled, we find that period detection becomes unreliable: we can only rely on crude summary statistics and contextual information to characterize these sources. In addition, some source classes yield non-period or multiply-periodic light curves, wherby the non-periodic features are expected in these cases to carry useful additional information not already contained in the periodic features. As an example, we apply metrics used in the time-domain study of quasars (Butler & Bloom 2010) to aid in disentangling the light curves of some complexly varying, long-period variables (e.g., semi-regular pulsating variables).

3. CLASSIFICATION FRAMEWORKS FOR VARIABLE STARS

The features extracted from a light curve give a characterization of the observed astronomical source. We need a rigorous way of turning this information into a probabilistic statement about the science class of that source. This is the goal of classification: given a set of sources whose science class is known, learn a model that describes each source's class probabilities as a function of its features. This model is then used to automatically predict the class probabilities, and the most likely science class, of each new source.

Several authors have used machine-learning methods to classify variable stars using their light curves: Brett et al. (2004) use Kohonen self-organizing maps, Eyer & Blake (2005) use the Bayesian mixture-model classifier `Autoclass` (Cheeseman & Stutz 1996) and Debosscher et al. (2007) experiment with several methods, including Gaussian mixture models, Bayesian networks, Bayesian averaging of artificial neural networks, and support vector machines. All of these methods have certainly enjoyed widespread use in the literature, and are a reasonable first set of tools to use in classifying variable stars. Our major contribution in this section is to introduce tree-based classification methods— including classification and regression trees (CART), random forests, and boosted trees—for the classification of variable stars. Tree-based classifiers are powerful because they are able to capture complicated interaction structure within the feature space, are robust to outliers, naturally handle multi-class problems, are immune to irrelevant features, easily cope with missing feature values, and are computationally efficient and scalable for large problems. Furthermore, they are simple to interpret and explain and generally yield accurate results. In §4 we show the superior performance of tree-based methods over the methods used in Debosscher et al. (2007) for classifying variable stars.

Below, we describe several tree-based classification approaches from the statistics and machine learning literature, showing how to train each classifier and how to predict science-class probabilities for each observed source. We also introduce a suite of pair-wise voting classifiers, where the multi-class problem of variable-star classification is simplified into a set of two-class problems and the results are aggregated to estimate class probabilities. Additionally, we outline a procedure for incorporating the known variable star class taxonomy into our classifier. Finally, we describe a rigorous risk-based framework to choose the optimal tuning parameter(s) for each classifier, and show how to objectively assess the expected performance of each classifier through cross-validation.

3.1. *Tree-based classifiers*

Decision tree learning has been a popular method for classification and regression in statistics and machine learning for more than 20 years (Breiman et al. 1984 popularized this approach). Recently, the astronomical community has begun to use tree-based techniques, with impressive results. For example, tree-based classifiers have been used by Suchkov et al. (2005) for SDSS object classification, by Ball et al. (2006) and O'Keefe et al. (2009) for star-galaxy separation, by Bailey et al. (2007) to identify supernova candidates, and by several groups for supernova classification in the recent DES Supernova Photometric Classification Challenge (Kessler et al. 2010).

Tree-based learning algorithms use recursive binary partitioning to split the feature space, $\mathcal{X}$, into disjoint regions, $R_1, R_2, ..., R_M$. Within each region, the response is modeled as a constant. Every split is performed with respect to one feature, producing a partitioning of $\mathcal{X}$ into a set of disjoint rectangles (nodes in the tree). At each step, the algorithm selects both the feature and split point that produces the smallest impurity in the two resultant nodes. The splitting process is repeated, recursively, on all regions to build a tree with multiple levels.

In this section we give an overview of three tree-based methods for classification: classification trees, random forest, and boosting. We focus on the basic concepts and a few particular challenges in using these classifiers for variable-star classification. For further details about these methods, we refer the interested reader to Hastie et al. (2009).

3.1.1. *Classification trees*

To build a classification tree, begin with a training set of (feature, class) pairs $(\mathbf{X}_1, Y_1), ..., (\mathbf{X}_n, Y_n)$, where Y_i can take any value in $\{1, ..., C\}$. At node m of the tree, which represents a region R_m of the feature space $\mathcal{X}$, the probability that a source with features in R_m belongs to class c is estimated by

$$\widehat{p}_{mc} = \frac{1}{N_m} \sum_{\mathbf{X}_i \in R_m} I(Y_i = c), \tag{8}$$

which is the proportion of the N_m training set objects in node m whose science class is c, where $I(Y_i = c)$ is the indicator function defined to be 1 if $Y_i = c$ and 0 else. In the tree-building process, each subsequent split is chosen amongst all possible features and split points to minimize a measure of the resultant node impurity, such as the Gini index ($\sum_{c \neq c'}^{C} \widehat{p}_{mc} \widehat{p}_{mc'}$) or entropy ($-\sum_{c=1}^{C} \widehat{p}_{mc} \log_2 \widehat{p}_{mc}$). The Gini index is the measure of choice for CART (Breiman et al. 1984), while entropy is used by the popular algorithm C4.5 (Quinlan 1996). This splitting process is repeated recursively until some pre-defined stopping criterion (such as minimum number of observations in a terminal node, or relative improvement in the objective function) is reached.

Once we have trained a classification tree on the examples $(\mathbf{X}_1, Y_1), ..., (\mathbf{X}_n, Y_n)$, it is simple to ingest features from a new instance, $\mathbf{X}_{\text{new}}$, and predict its science class. Specifically, we first identify which tree partition $\mathbf{X}_{\text{new}}$ resides in, and then assign it a class based on that node's estimated probabilities from (8). For example, if $\mathbf{X}_{\text{new}} \in R_m$, then the classification-tree probability that the source is in class c is

$$\widehat{p}_c(\mathbf{X}_{\text{new}}) = \widehat{p}_{mc} \tag{9}$$

where $\widehat{p}_{mc}$ is defined in (8). Using (9), the predicted science class is $\widehat{p}(\mathbf{X}_{\text{new}}) = \arg\max_c \widehat{p}_c(\mathbf{X}_{\text{new}})$. Note that we are free to describe the classification output for each new source either as a vector of class probabilities or as its predicted science class.

There remains the question of how large of a tree should be grown. A very large tree will fit the training data well, but will not generalize well to new data. A very small tree will likely not be large enough to capture the complexity of the data-generating process. The appropriate size of a tree ultimately depends on the complexity of model necessary for the particular application at hand, and hence should be determined by the data. The standard approach to this problem is to build a large tree, T, with M terminal nodes and then to *prune* this tree to find the subtree T^* of T that minimizes a cross-validation estimate of its statistical risk (see §3.5).

3.1.2. *Random forest*

Classification trees are simple, yet powerful, non-parametric classifiers. They work well even when the true model relating the feature space to the class labeling is complicated, and generally yield estimates with very small bias. However, tree models tend to have high variance. Small changes in the training set features can produce very different estimated tree structure. This is a by-product of the hierarchical nature of the tree model: small differences in the top few nodes of a tree can produce wildly different structure as those perturbations are propagated down the tree. To reduce the variance of tree estimates, *bagging* (bootstrap aggregation, Breiman 1996) was proposed to average the predictions of B trees fitted to bootstrapped samples of the training data. *Random forest* (Breiman 2001) is an improvement to bagging that attempts to de-correlate the B trees by selecting a random subset of m_{try} of the input features as candidates for splitting at each node during the tree-building process. The net result is that the final, averaged random forest model has lower variance than the bagging model, while maintaining a small bias (see Hastie et al. 2009, ch.15 for a discussion).

To obtain a random forest classification model, we grow B de-correlated classification trees. For a new variable star, the class probabilities are estimated as the proportion of the B trees that predict each class. As in classification trees, we are free to describe each source as a vector of class probabilities or a best-guess class. This prescription generally works well because by averaging the predictions over many bootstrapped trees, the estimated probabilities are more robust to chance variations in the original training set, and are almost always more accurate than the output of a single tree. Another advantage to random forest is the relative robustness of the estimates to choices of the tuning parameters (B, m_{try}, and the size of each tree) compared to other non-parametric classification techniques. In practice, we use the parameter values that give minimal cross-validation risk.

3.1.3. *Boosted trees*

Boosting is a method of aggregating simple rules to create a predictive model whose performance is 'boosted' over that of any of its ensemble members (Freund & Schapire 1996). In classification boosting, a sequence of simple classifiers (referred to as weak-learners) is applied, whereby in each iteration the training observations are re-weighted so that those sources which are repeatedly misclassified are given greater influence in the subsequent classifiers. Therefore, as the iterations proceed, the classifier pays more attention to data points that are difficult to classify, yielding improved overall performance over that of each weak-learner. The predicted class probabilities are obtained from a weighted estimate of the individual classifiers, with weights proportional to the accuracy of each classifier.

Classification trees are natural base learners in a boosting algorithm because of their simplicity, interpretability, and ability to deal with data containing outliers and missing values. Moreover, there are efficient algorithms that can quickly estimate boosted trees using gradient boosting (Friedman 2001). It is usually sufficient to use single-split trees (so-called decision stumps) as base-learners, though in situations with more complicated interactions, bigger trees are necessary. We use the training data to choose this tuning parameter through cross-validation.

3.2. *Measuring feature importance*

An additional advantage to tree-based classifiers is that, because the trees are constructed by splitting one feature at a time, they allow us to estimate the importance of each feature in the model. A feature's importance can be deduced by, for instance, counting how often that feature is split or looking at the resultant decrease in node impurity for splits on that feature. Additionally, random forest provides a measure of the predictive strength of each feature, referred

to as the *variable importance*, which tells us roughly what the decrease in overall classification accuracy would be if a feature were replaced by a random permutation of its values. Random forest has a rapid procedure for estimating variable importance via its *out-of-bag* samples for each tree, those data that were not included in the bootstrapped sample.

Analyzing the feature importance is a critical step in building an accurate classification model. By determining which features are important for distinguishing certain classes, we gain valuable insight into the physical differences between particular science classes. Moreover, we can visualize which types of features are more predictive than others, which can inform the use of novel features or the elimination of useless features in a second-generation classifier.

3.3. *Pairwise classifiers*

A common approach for multi-class classification is to reduce the C-class problem into a set of $C(C-1)/2$ pairwise comparisons. This is a viable approach because two-class problems are usually easier to solve since the class boundaries tend to be relatively simple. Moreover, some classification methods, such as support vector machines (SVM, Vapnik 2000), are designed to work only on two-class problems. In pairwise classification, classifiers for all $C(C-1)/2$ two-class problems are constructed. The challenge, then, is to map the output from the set of pairwise classifiers for each source (pairwise probabilities or class indicators) to a vector of C class probabilities that accurately reflects the science class of that source. This problem is referred to as pairwise coupling.

The simplest method of pairwise coupling is voting (Knerr et al. 1990; Friedman 1996), where the class of each object is determined as the winner in a pairwise head-to-head vote. Pairwise voting is suboptimal because it ignores the pairwise class probabilities and tends to estimate inaccurate C-class probabilities. In situations where pairwise class probability estimates are available, voting is outperformed by other methods such as the Kullback-Leibler based technique of Hastie & Tibshirani (1998) and the approaches of Wu et al. (2004), which reduce the problem to solving a linear system of equations. In this paper, we explore the use of both tree-based classifiers and SVMs in pairwise classifiers. To obtain C-class probabilities, we employ the second pairwise coupling method introduced by Wu et al. (2004). We refer the interested reader to that paper for a more detailed description of the method and a review of similar techniques in the literature.

3.4. *Hierarchical classification*

In variable star classification, we have at our disposal a well-established hierarchical taxonomy of classes based on the physics and phenomenology of these stars and stellar systems. For instance, at the top level of our taxonomy, we can split the science classes into three main categories: pulsating, eruptive, and multi-star systems. From there, we can continue to divide the sub-classes until we are left with exactly one of the original 25 science classes in each node (see figure 2). For classification purposes, the meaning of the hierarchy is clear: mistakes at the highest levels of the hierarchy are more costly than mistakes made at deeper levels because the top levels of the hierarchy divide physical classes that are considerably different, whereas deeper levels divide subclasses that are quite similar.

Incorporating a known class hierarchy, such as that of figure 2, into a classification engine is a research field that has received much recent attention in the machine learning literature (see Silla & Freitas 2011 for a survey of these methods). By considering the class hierarchy, these classifiers generally outperform their 'flat classifier' counterparts because they impose higher penalties on the more egregious classification errors. In this paper, we consider two types of hierarchical classification approaches: HSC (hierarchical single-label classification, Cesa-Bianchi et al. 2006) and HMC (hierarchical multi-label classification, Blockeel et al. 2006). We implement both HSC and HMC using random forests of decision trees. Below, we provide a synopsis of HSC and HMC. For more details about these methods, see Vens et al. (2008).

In HSC, a separate classifier is trained at each non-terminal node in the class hierarchy, whereby the probabilities of each classifier are combined using conditional probability rules to obtain each of the class probabilities. This has a similar flavor to the pairwise classifier approach of §3.3, but by adhering to the class hierarchy it need only build a small set of classifiers and can generate class probabilities in a straight-forward, coherent manner. Moreover, different classifiers and/or sets of features can be used at each node in HSC, allowing for the use of more general classifiers at the top of the hierarchy and specialized domain-specific classifiers deeper in the hierarchy. A recent paper of Blomme et al. (2010) applied a method similar to HSC, using Gaussian mixture classifiers, to classify variable stars observed by the *Kepler* satellite. A second hierarchical classification approach is HMC, which builds a single classifier in which errors on the higher levels of the class hierarchy are penalized more heavily than errors deeper down the hierarchy. In the version of HMC that we use, the weight given to a classification error at depth d in the class hierarchy is w_0^d, where $w_0 \in (0, 1)$ is a tuning parameter. This forces the algorithm to pay more attention to the top level, minimizing the instances of catastrophic error (defined in §4.3).

3.5. *Classifier assessment through cross-validation*

We have introduced a few methods that, given a sample of training data, estimate a classification model, $\widehat{p}$, to predict the science class of each new source. In this section, we introduce statistically-rigorous methodology for assessing each classifier and choosing the optimal classifier amongst a set of alternatives. Since our ultimate goal is to accurately classify newly-collected data, we will use the classifier that gives the best expected performance on new data. We achieve this by defining a classifier's *statistical risk* (i.e. prediction error) and computing an unbiased estimate of that risk via *cross-validation*. We will ultimately use the model that obtains the smallest risk estimate.
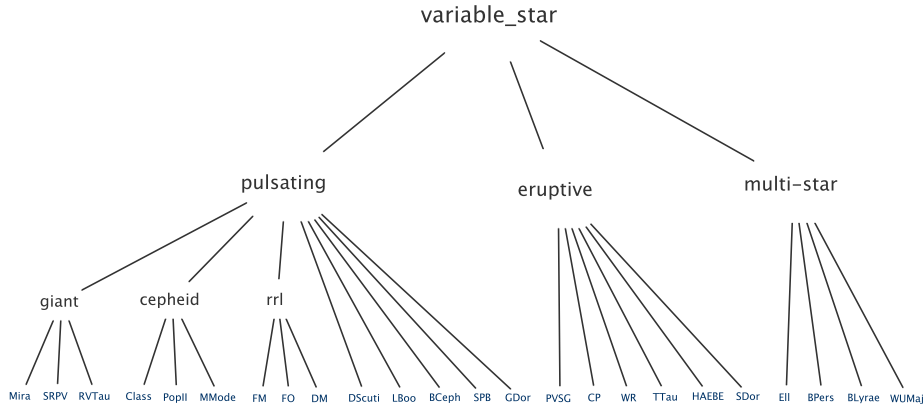
FIG. 2.— Variable star classification hierarchy for the data used in §4. This structure is a crucial element of the two hierarchical classifiers used in this study, HSC and HMC. The hierarchy is constructed based on knowledge of the physical processes that govern each type of object. At the top level, the sources split into three major categories: pulsating, eruptive, and multi-star systems.

Given a new source of class Y, having features $\mathbf{X}$, we define a loss function, $L(Y, \widehat{p}(\mathbf{X}))$, describing the penalty incurred by the application of our classifier, $\widehat{p}$, on that source. The loss function encompasses our notion of how much the classifier $\widehat{p}$ has erred in predicting the source's class from its features $\mathbf{X}$. The expected value of L, $E[L(Y, \widehat{p}(\mathbf{X}))]$, is the statistical risk, $R(\widehat{p})$, of the classifier. The expected value, $E[\cdot]$, averages over all possible realizations of $(\mathbf{X}, Y)$ to tell us how much loss we can expect to incur for the predicted classification of each new source (under the assumption that new data are drawn from the same distribution as the training data). A key aspect to this approach is that it guards against over-fitting to the training data: if a model is overly complex, it will only add extra variability in classification without decreasing the bias of the classifier, leading to an increase in the risk (this is the bias-variance tradeoff, see Wasserman 2006).

Conveniently, within this framework each scientist is free to tailor the loss function to meet their own scientific goals. For instance, an astronomer interested in finding Mira variables could define a loss function that incurs higher values for mis-classified Miras. In this work, we use the vanilla 0-1 loss that is defined to be 0 if $Y = \widehat{p}(\mathbf{X})$ and 1 if misclassified (here, $\widehat{p}(\mathbf{X})$ is the estimated class of the source; alternatively, we could define a loss function over the set of estimated class probabilities, $\{\widehat{p}_1(\mathbf{X}), ..., \widehat{p}_C(\mathbf{X})\}$). Under 0-1 loss, the statistical risk of a classifier is its expected overall misclassification rate, which we aim to minimize.

There remains the problem of how to estimate the statistical risk, $R(\widehat{p})$ of a classifier $\widehat{p}$. If labeled data were plentiful, we could randomly split the sources into training and validation sets, estimating $\widehat{p}$ with the training set and computing a risk estimate $\widehat{R}(\widehat{p})$ with the validation set. Since our data are relatively small in number, we use k-fold cross-validation to estimate R. In this procedure, we first split the data into K (relatively) equal-sized parts. For each subset $k = 1, ..., K$ the classifier is fitted on all of the data not in k and a risk estimate, $\widehat{R}_{(-k)}(\widehat{p})$, is computed on the data in set k. The cross-validation risk estimate is defined as $\widehat{R}_{\mathrm{CV}}(\widehat{p}) = \frac{1}{K} \sum_{k=1}^{K} \widehat{R}_{(-k)}(\widehat{p})$. As shown in Burman (1989), for $K \gtrsim 4$, $\widehat{R}_{\mathrm{CV}}(\widehat{p})$ is an approximately-unbiased estimate of $R(\widehat{p})$. In this paper, we use $K = 10$ fold cross-validation.

In addition to selecting between different classification models, cross-validation risk estimates can be used to choose the appropriate tuning parameter(s) for each classifier. For instance, we use cross-validation to choose the optimal pruning depth for classification trees, to pick the optimal number and depth of trees to build, and number of candidate splitting features to use at each split for random forests, and to select the optimal size of the base learner, number of trees, and learning rate for boosted decision trees. The optimal set of tuning parameters for each method is found via a grid search. For each of the methods considered, we find that $\widehat{R}_{\mathrm{CV}}$ is stable in the neighborhood of the optimal tuning parameters, signifying that the classifiers are relatively robust to the specific choice of tuning parameters and that a grid search over those parameters is sufficient to obtain near-optimal results.

4. CLASSIFIER PERFORMANCE ON OGLE+HIPPARCOS DATA SET

4.1. *Description of data*

In this paper, we test our feature extraction and classification methods using a mixture of variable star photometric data from the OGLE and Hipparcos surveys. OGLE (Optical Gravitational Lensing Experiment, Udalski et al. 1999)

TABLE 1
Dataset characteristics, by survey.

Survey	NLC[a]	%NLC$_{deb}$[b]	NLC used[c]	$\langle T_{tot} \rangle$ (days)[d]	$\langle N_{epochs} \rangle$
HIPPARCOS	1044	100.0	1019	1097	103
OGLE	523	99.2	523	1067	329

[a] Total number of light curves available to us.
[b] Percentage of Debosscher et al. (2007) light curves available to us.
[c] Number of light curves after removal of sources with ambiguous class and exclusion of small classes.
[d] Average time baseline.

TABLE 2
Dataset characteristics, by science class.

Variable Star Class	Name$_{deb}$[a]	NLC[b]	%NLC$_{deb}$	Instrument	$\langle N_{epochs} \rangle$	$min(f_1)$[c]	$\langle f_1 \rangle$[c]	$max(f_1)$[c]
a. Mira	MIRA	144	100.0	HIPPARCOS	98	0.0020	0.09	11.2508
b. Semireg PV	SR	42	100.0	HIPPARCOS	99	0.0010	0.15	1.0462
c. RV Tauri	RVTAU	6	46.2	HIPPARCOS	104	0.0012	0.05	0.1711
d. Classical Cepheid	CLCEP	191	97.9	HIPPARCOS	108	0.0223	0.15	0.4954
e. Pop. II Cepheid	PTCEP	23	95.8	HIPPARCOS	107	0.0037	0.21	0.7648
f. Multi. Mode Cepheid	DMCEP	94	98.9	OGLE	181	0.5836	1.21	1.7756
g. RR Lyrae, FM	RRAB	124	96.1	HIPPARCOS	91	1.2149	1.95	9.6197
h. RR Lyrae, FO	RRC	25	86.2	HIPPARCOS	92	2.2289	3.15	4.3328
i. RR Lyrae, DM	RRD	57	100.0	OGLE	304	2.0397	2.61	2.8177
j. Delta Scuti	DSCUT	114	82.0	HIPPARCOS	129	0.0044	7.90	19.7417
k. Lambda Bootis	LBOO	13	100.0	HIPPARCOS	84	7.0864	12.36	19.8979
l. Beta Cephei	BCEP	39	67.2	HIPPARCOS	96	0.0014	4.94	10.8319
m. Slowly Puls. B	SPB	29	61.7	HIPPARCOS	101	0.1392	1.09	11.8302
n. Gamma Doradus	GDOR	28	80.0	HIPPARCOS	95	0.2239	2.24	9.7463
o. Pulsating Be	BE	45	78.9	HIPPARCOS	106	0.0011	2.12	14.0196
p. Per. Var. SG	PVSG	55	72.4	HIPPARCOS	102	0.0015	3.41	15.7919
q. Chem. Peculiar	CP	51	81.0	HIPPARCOS	105	0.0076	2.57	13.4831
r. Wolf-Rayet	WR	41	65.1	HIPPARCOS	99	0.0011	6.56	19.2920
s. T Tauri	TTAU	14	82.4	HIPPARCOS	67	0.0013	1.85	11.2948
t. Herbig AE/BE	HAEBE	15	71.4	HIPPARCOS	83	0.0009	1.41	10.0520
u. S Doradus	LBV	7	33.3	HIPPARCOS	95	0.0008	0.20	0.5327
v. Ellipsoidal	ELL	13	81.2	HIPPARCOS	105	0.1070	1.37	3.5003
w. Beta Persei	EA	169	100.0	OGLE	375	0.0127	0.93	3.1006
x. Beta Lyrae	EB	145	98.6	OGLE	365	0.0175	0.71	4.5895
y. W Ursae Maj.	EW	58	98.3	OGLE	369	0.2232	2.44	8.3018

[a] Class name in Debosscher et al. (2007).
[b] Total number of light curves used, after removal of ambiguous sources.
[c] f_1 is the frequency of the first harmonic in day^{-1}.

is a ground-based survey from Las Campanas Observatory covering fields in the Magellanic Clouds and Galactic bulge. Hipparcos Space Astrometry Mission (Perryman et al. 1997) was an ESA project designed to precisely measure the positions of more than one hundred thousand stars. The data selected for this paper are the OGLE and Hipparcos sources analyzed by Debosscher et al. (2007), totaling 90% of the variable stars studied in that paper. A summary of the properties, by survey, of the data used in our study, is in table 1. The light curve data and classifications used for each source can be obtained through our `dotastro.org` light curve repository.[8]

This sample was designed by Debosscher et al. (2007) to provide a sizable set of stars within each science class, for a broad range of classes. Our sample contains stars from the 25 science classes analyzed in their paper. Via an extensive literature search, they obtained a set of confirmed stars of each variability class. In table 2 we list, by science class, the proportion of stars in that data set that we have available for this paper. Since the idea of their study was to capture and quantify the typical variability of each science class, the light curves were pre-selected to be of good quality and to have an adequate temporal sampling for accurate characterization of each science class. For example, the multi-mode Cepheid and double-mode RR Lyrae stars, which have more complicated periodic variability, were sampled from OGLE because of its higher sampling rate.

In our sample, there are 25 objects that are labeled as two different science classes. Based on a literature search of these stars, we determine that 14 of them reasonably belong to just a single class (5 S Doradus, 2 Herbig AE/BE, 3 Wolf Rayet, 2 Delta Scuti, 1 Mira, and 1 Lambda Bootis). The other 11 doubly-labeled stars, which are listed in table 6, were of an ambiguous class or truly belonged to two different classes, and were removed from the sample. See Appendix B for a detailed analysis and references for the doubly-labeled objects. Because the sample was originally constructed by Debosscher et al. (2007) to consist only of well-understood stars with confident class labeling, we are justified in excluding these sources.

[8] http://dotastro.org/lightcurves/project.php?Project_ID=123

TABLE 3
PERFORMANCE OF CLASSIFIERS ON OGLE+HIPPARCOS DATA SET,
AVERAGED OVER 10 REPETITIONS.

Method	Misclassification %[a]	Catastrophic error %[a]	CPU[b]
CART	32.2	13.7	10.6
C4.5	29.8	12.7	14.4
RF	**22.8**	8.0	117.6
Boost	25.0	9.9	466.5
CART.pw	25.8	8.7	323.2
RF.pw	23.4	8.0	290.3
Boost.pw	24.1	8.2	301.5
SVM.pw	25.3	8.4	273.0
HSC-RF	23.5	**7.8**	230.9
HMC-RF	23.4	8.2	946.0

[a] Estimated using 10-fold cross-validation.
[b] Average processing time in seconds for 10-fold cross-validation on a 2.67 GHz Macintosh with 4 GB of RAM.

4.2. *Class-wise distribution of light-curve features*

Using the methodology in §2, we estimate features for each variable star in the data set using their light curve. The feature-extraction routines take 0.8 seconds per light curve, giving us a 53-dimensional representation of each variable star. The computations are performed in Python and C using a non-parallelized, single thread on a 2.67 GHz Intel Xeon X5550 CPU running on a v2.6.18 linux kernel machine. We estimate that the periodic-feature routines account for 75% of the computing time and scale linearly with the number of epochs in the light curve. Note that these metrics do not take into account the CPU time needed to read the XML data files from disk and load the data into memory.

Plots of 1-dimensional density estimates, by science class, of a selected set of features are in figure 3. These class-wise feature distributions allow us to quickly and easily identify the differences, in feature space, between individual variable star science classes. Density plots are very useful for this visualization because they provide a complete feature-by-feature characterization of each class, showing any multi-modality, outliers, and skewness in the feature distributions. For instance, it is immediately obvious that several of the eruptive-type variable star classes have an apparent bi-modal or relatively flat frequency distributions, likely attributed to their episodic nature. Conversely, the RR Lyrae frequency distributions are all narrow and peaked, showing that indeed these stars are well-characterized by the frequency of their flux oscillations. The feature density plots also inform us of which feature(s) are important in separating different sets of classes. For example, the RR Lyrae, FO and RR Lyrae, DM stars have overlapping distributions for each of the features in figure 3 except the feature QSO, where their distributions are far apart, meaning that QSO will be a useful classification feature in separating stars of those two classes.

4.3. *Classifier comparison*

In this section, we compare the different classification methods introduced in §3. To fit each classifier, except HMC-RF, we use the statistical environment R[9]. To fit HMC-RF we use the open-source decision tree and rule learning system Clus.[10] Each of the classifiers was tuned via a grid search over the relevant tuning parameters to minimize the cross-validation misclassification rates. To evaluate each classifier, we consider two separate metrics: the overall misclassification error rate and the catastrophic error rate. We define catastrophic errors to be any classification mistake in the top-level of the variable-star hierarchy in figure 2 (i.e., pulsating, eruptive, multi-star). The performance measures for each classifier, averaged over 10 cross-validation trials, are listed in table 3. In terms of overall misclassification rate, the best classifier is a random forest with $B = 1000$ trees, achieving a 22.8% average misclassification rate. In terms of catastrophic error rate, the HSC-RF classifier with $B = 1000$ trees achieves the lowest value, 7.8%. The processing time required to fit the ensemble methods is greater than the time needed to fit single tree models. However, this should not be viewed as a limiting factor: once any of these models is fit, predictions for new data can be produced very rapidly. For example, for a random forest classifier of 1000 trees, class probability estimates can be generated for new data at the rate of 3700 instances per second.

4.3.1. *Tree-based classifiers*

On average, the single-tree classifiers–CART and C4.5–are outperformed by the tree ensemble methods–random forest and tree boosting–by 21% in terms of misclassification error rate. The classification performances of the single-tree classifiers are near that of the best classifier in Debosscher et al. (2007), which achieves a 30% error rate. Tree-based classifiers seem particularly adept at variable-star classification, and ensembles of trees achieve impressive results. Single trees take on the order of 10 seconds to fit a model, prune based on cross-validation complexity, and predict classification labels for test cases. Tree ensemble methods take 10-40 times longer to fit 1000 trees. Overall, the random forest classifier is the best classification method for these data: it achieves the lowest overall misclassification rate, low catastrophic error rate, and is the third fastest algorithm.

[9] R is a freely-available language and environment for statistical computing and graphics available at http://cran.r-project.org/
[10] http://dtai.cs.kuleuven.be/clus/index.html

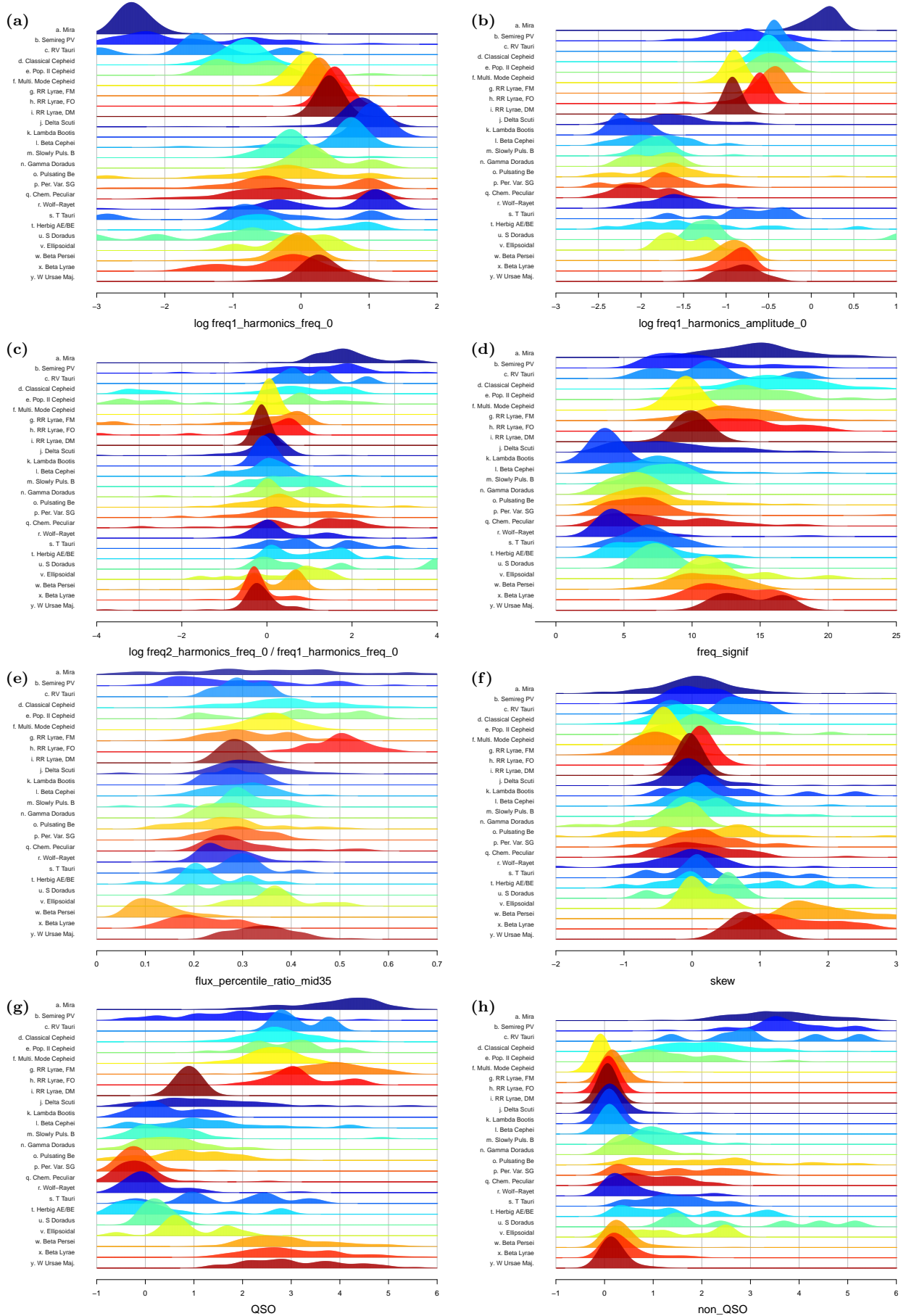FIG. 3.— Histograms of several features, by class. The features plotted are (a) the first frequency in cycles/day, (b) amplitude of the first frequency in mag, (c) the ratio of the second to the first frequencies, (d) statistical significance of the periodic model, (e) flux ratio middle 35th to middle 95th quantiles, (f) flux skew, (g) Butler & Bloom 2010 QSO variability, and (h) Butler & Bloom 2010 non-QSO variability.

4.3.2. *Pairwise classifiers*

We implement four pairwise classifiers: CART, random forest, boosted trees, and SVM. Of these, random forest achieves the best results in terms of both misclassification rate and catastrophic error rate, at 23.4% and 8.0%, respectively. The pairwise classifiers all perform better than single-tree classifiers but tend to fare worse than the single random forest method. It is interesting to note that our implementation of SVM achieves a 25.3% misclassification rate, a vast improvement over the 50% SVM misclassification rate found by Debosscher et al. (2007). This is likely due to both our use of better features and our pre-selection of the 25 features (chosen via cross-validation) with highest random-forest variable importance for use in the SVM. Unlike tree models, SVM is not immune to the inclusion of many useless features; when we include all 53 features into the SVM, our error rate skyrockets to 54%.

4.3.3. *Hierarchical classifiers*

Two of our classifiers, HSC-RF and HMC-RF, incorporate the hierarchical class taxonomy when building a classifier. Both of these methods achieve overall classification error rates slightly worse (sub-1% level) than that of the random forest classifier, while HSC-RF reaches the best overall catastrophic error rate (7.8%). HMC-RF slightly outperforms HSC-RF with respect to misclassification rate, but its current implementation takes 4 times as much CPU time. HSC-RF, HMC-RF, pairwise random forest and the original random forest are the best methods in terms of error rates, but random forest is at least twice as fast as any of the other methods.

4.4. *Direct comparison to Debosscher et al. (2007)*

Random forest achieves a 22.8% average misclassification rate, a 24% improvement over the 30% misclassification rate achieved by the best method of Debosscher et al. (2007) (Bayesian model averaging of artificial neural networks). Furthermore, each of the classifiers proposed in this paper, except the single-tree models CART and C4.5, achieves an average misclassification rate smaller than 25.8% (see table 3). There is no large discrepancy between the different ensemble methods—the difference between the best (random forest) and worst (boosting) ensemble classifier is 2.2%, or an average of 34 more correct classifications—but in terms of both accuracy and speed, random forest is the clear winner.

In comparing our results to the Debosscher et al. (2007) classification results, it is useful to know whether the gains in accuracy are due to the use of better classifiers, more accurate periodic feature extraction, informative non-periodic features, or some combination of these. To this end, we classify these data using the following sets of features:

1. The periodic features estimated by Debosscher et al. (2007).

2. Our estimates of the periodic features following §2.

3. The non-periodic features proposed in §2

4. The non-periodic features in addition to our periodic features.

Misclassification rates from the application of our classifiers to the above sets of features are plotted in figure 4. As a general trend, using both our periodic and non-periodic features is better than using only our periodic features, which is in turn better than using Debosscher et al.'s periodic features, which achieves similar rates to using only the non-periodic features. Using a random forest classifier, we find that the average cross-validated misclassification rates are 22.8% using all features, 23.8% using our periodic features, 26.7% using Debosscher et al. (2007) features, and 27.6% using only our non-periodic features. This is evidence that we obtain better classification results both because our classification model is better and because the extracted features we use are more informative.

4.5. *Analysis of classification errors*

Understanding the source and nature of the mistakes that our classifier makes can alert to possible limitations in the classification methods and feature extraction software and aid in the construction of a second-generation light-curve classifier. Let us focus on the classifier with best overall performance: the random forest, whose cross-validated misclassification rate was 22.8%. In figure 5 we plot the confusion matrix of this classifier, which is a tabular representation of the classifier's predicted class versus the true class. A perfect classifier would place all of the data on the diagonal of the confusion matrix; any deviations from the diagonal inform us of the types of errors that the classifier makes.

A few common errors are apparent in figure 5. For instance, Lambda Bootis and Beta Cephei are frequently classified as Delta Scuti. Wolf-Rayet, Herbig AE/BE and S Doradus stars are usually classified as Periodic Variable Super Giants, and T Tauri are often misclassified as Semiregular Pulsating Variables. None of these mistakes are particularly egregious: often the confused science classes are physically-similar. Also, the mis-classified examples often come from classes with few training examples (see below) or characteristically low-amplitude objects (see §4.8).

As the random forest is a probabilistic classifier, for each source it supplies us with a probability estimate that the source belongs to each of the science classes. Until now, we have collapsed each vector of probabilities into an indicator of most probable class, but there is much information available to extract from the individual probabilities. For instance, in figure 6 we plot, by class, the random-forest estimated probability that each source is of its true class. We immediately see a large disparity in performance between the classes: for a few classes, we estimate high probabilities of true class, while for others we generally estimate low probabilities. This discrepancy is related to the
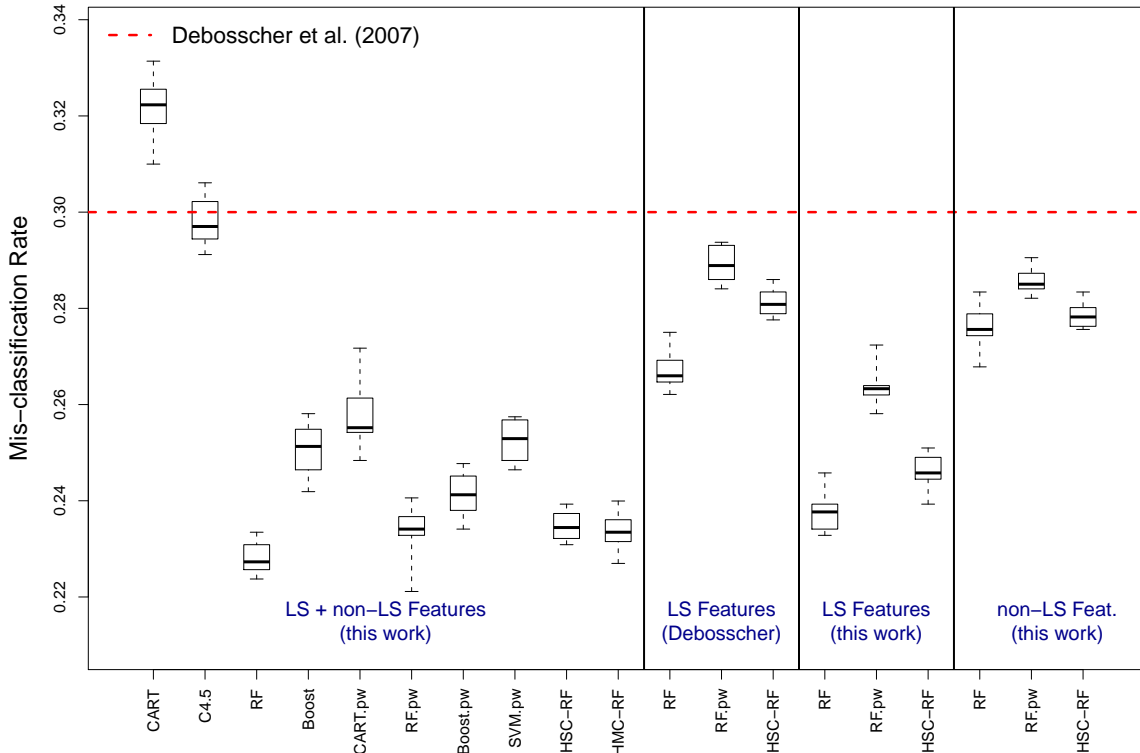
FIG. 4.— Distribution of cross-validation error rates for several classifiers on the OGLE+Hipparcos data, obtained from 10 repetitions. The classifiers are divided based on the features on which they were trained; from left to right: (1) all of the periodic and non-periodic features that we estimate, (2) the Lomb-Scargle features estimated by Debosscher et al. (2007), (3) the Lomb-Scargle features estimated by us, and (4) the non-periodic features. In terms of mis-classification rate, the classifiers trained on all of our features perform the best, followed by those trained only on our periodic features, those trained on Debosscher et al.'s periodic features, and those trained on only the non-periodic features. All of the classifiers used, except single trees, achieve better error rates than the best classifier from Debosscher et al. (dashed line).

size of each class: within the science classes that are data-rich, we tend to get the correct class, while in classes with scarce data, we usually estimate the wrong class. This same effect is seen in Debosscher et al. (2007), (their table 5). This is a common problem in statistical classification for unbalanced class sizes: classifiers such as random forest try to minimize the overall classification rate, thus focusing most of their efforts on the larger classes. One can remedy this by weighting the training data inversely proportional to their class size. However, the price to pay for the increase in balanced error among the classes is a higher overall misclassification rate (see Breiman et al. 1984). The better solution is obviously to obtain more training examples for the under-sampled classes to achieve a better characterization of these classes.

We have experimented with a random forest classifier using inverse class-size weighting. The results of this experiment were as expected: our overall misclassification rate climbs to 28.0%, a 23% increase in error over the standard random forest, but we perform better within the smaller classes. Notably, the number of correctly-classified Lambda Bootis increases from 1 to 7, while the number of correctly-classified Ellipsoidal variables jumps from 6 to 11, Beta Cephei from 5 to 23, and Gamma Doradus from 8 to 15. All four classes in which the original random forest found no correct classifications each had at least two correct classifications with the weighted random forest.

4.6. *Performance for specific science classes*

Although our classifier was constructed to minimize the number of overall misclassifications in the 25-class problem, we can also use it to obtain samples of objects from science classes of interest via probability thresholding. The random forest classifier produces a set of class-wise posterior probability estimates for each object. To construct samples of a particular science class, we define a threshold on the posterior probabilities, whereby any object with class probability estimate larger than the threshold is included in the sample. By decreasing the threshold, we trade off purity of the sample for completeness, thereby mapping out the receiver operating characteristic (ROC) curve of the classifier.

In figure 7, we plot the cross-validated ROC curve of the multi-class random forest for four different science classes: (a) RR Lyrae, FM, (b) T Tauri, (c) Milky Way Structure, which includes all Mira, RR Lyrae, and Cepheid stars, and (d) Eclipsing Systems, which includes all Beta Persei, Beta Lyrae, and W Ursae Major stars. Each ROC curve shows the trade-off between the efficiency and purity of the samples. At a 95% purity, the estimated efficiency for RR Lyrae, FM is 94.7%, for Milky Way Structure stars 98.2%, and for Eclipsing Systems 99.1%. The T Tauri ROC curve is substantially worse than these other classes due to the small number of sources (note: inverse class-size weighting does not help in this problem because the ordering of the posterior class probabilities drives the ROC curve, not the

True Class

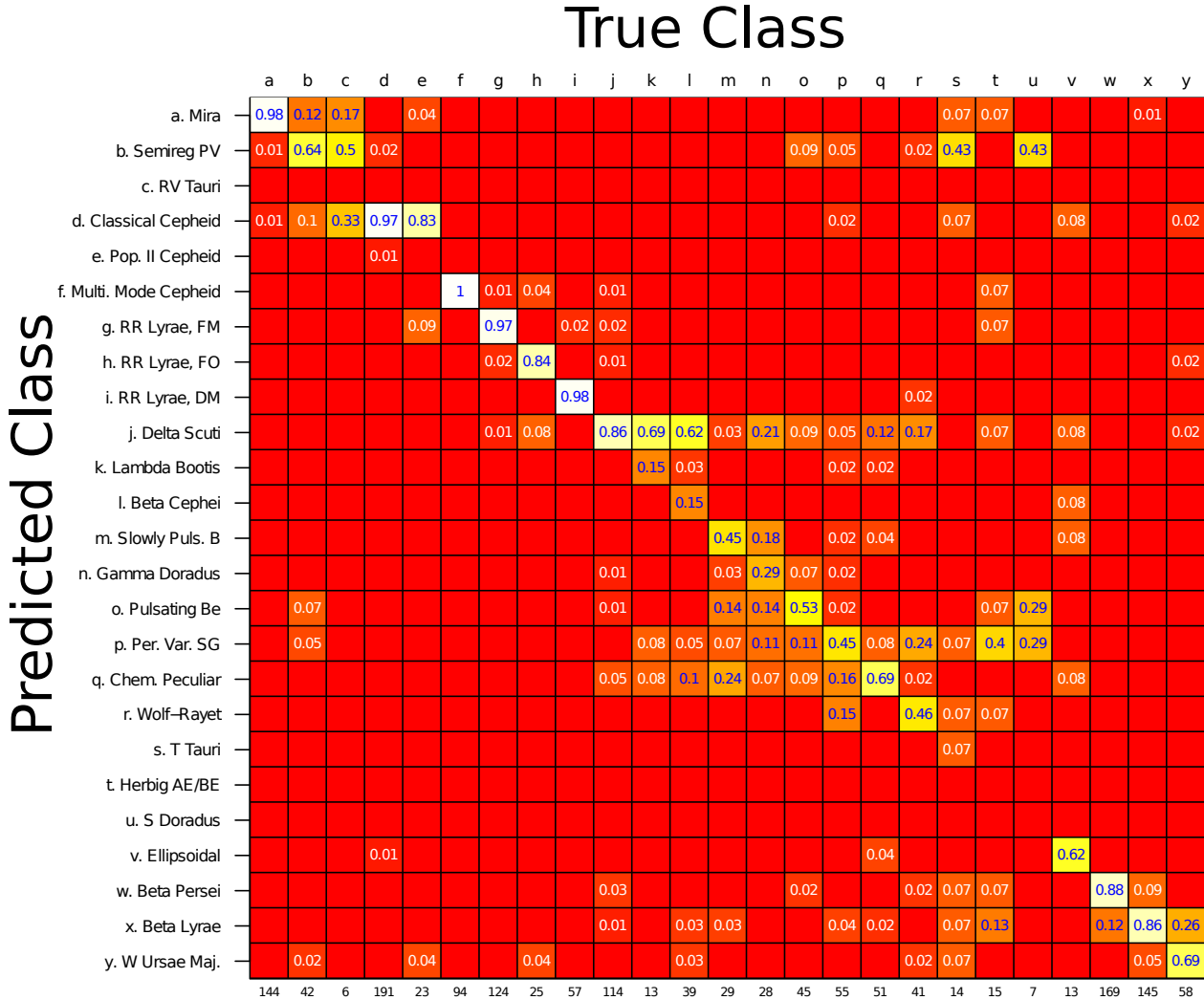| Predicted Class	a	b	c	d	e	f	g	h	i	j	k	l	m	n	o	p	q	r	s	t	u	v	w	x	y
a. Mira	0.98	0.12	0.17		0.04														0.07	0.07			0.01		
b. Semireg PV	0.01	0.64	0.5	0.02										0.09	0.05		0.02		0.43		0.43				
c. RV Tauri																									
d. Classical Cepheid	0.01	0.1	0.33	0.97	0.83										0.02		0.07				0.08				0.02
e. Pop. II Cepheid				0.01																					
f. Multi. Mode Cepheid						1	0.01	0.04		0.01									0.07						
g. RR Lyrae, FM					0.09		0.97		0.02	0.02									0.07						
h. RR Lyrae, FO							0.02	0.84		0.01															0.02
i. RR Lyrae, DM									0.98									0.02							
j. Delta Scuti							0.01	0.08		0.86	0.69	0.62	0.03	0.21	0.09	0.05	0.12	0.17		0.07		0.08			0.02
k. Lambda Bootis											0.15	0.03			0.02	0.02									
l. Beta Cephei												0.15										0.08			
m. Slowly Puls. B													0.45	0.18		0.02	0.04					0.08			
n. Gamma Doradus										0.01			0.03	0.29	0.07	0.02									
o. Pulsating Be		0.07								0.01			0.14	0.14	0.53	0.02				0.07	0.29				
p. Per. Var. SG		0.05									0.08	0.05	0.07	0.11	0.11	0.45	0.08	0.24	0.07	0.4	0.29				
q. Chem. Peculiar										0.05	0.08	0.1	0.24	0.07	0.09	0.16	0.69	0.02				0.08			
r. Wolf–Rayet																0.15		0.46	0.07	0.07					
s. T Tauri																			0.07						
t. Herbig AE/BE																									
u. S Doradus																									
v. Ellipsoidal				0.01													0.04					0.62			
w. Beta Persei										0.03					0.02			0.02	0.07	0.07			0.88	0.09	
x. Beta Lyrae										0.01		0.03	0.03			0.04	0.02		0.07	0.13			0.12	0.86	0.26
y. W Ursae Maj.		0.02			0.04		0.04			0.03						0.02			0.07					0.05	0.69
	144	42	6	191	23	94	124	25	57	114	13	39	29	28	45	55	51	41	14	15	7	13	169	145	58

FIG. 5.— Cross-validated confusion matrix obtained by the random forest classifier for the OGLE+Hipparcos data. A perfect classifier would place all mass on the diagonal. We have sorted the science classes by physical similarity, so large numbers near the diagonal signify that the classifier is performing well. On average, the classifier performs worse on the eruptive events, as exemplified by a large spread of mass for classes p through u. The overall error rate for this classifier was 21.1%.

magnitude of those probabilities). Surprisingly, the 25-class random forest ROC curve dominates the ROC curve of a one-versus-all random forest for three of the four science classes, with vastly superior results for small classes. This implies that our approach of predicting all class probabilities with one classifier is better than constructing a separate classifier for each science class of interest.

4.7. Feature importance

In §3.2, we described how to estimate the importance of each feature in a tree-based classifier. In figure 8, the importance of each feature from a pairwise random forest classifier is plotted, by class. The intensity of each pixel depicts the proportion of instances of each class that are correctly-classified by using each particular feature in lieu of a feature containing random noise. The intensities have been scaled to have the same mean across classes to mitigate the effects of unequal class sizes and are plotted on a square-root scale to decrease the influence of dominant features. In independently comparing the performance of each feature to that of noise, the method does not account for correlations amongst features. Consequentially, sets of features that measure similar properties–e.g. `median_absolute_deviation`, `std`, and `stetson_j` are all measures of the spread in the fluxes–may each have high importance, even though their combined importance is not much greater than each of their individual importances.

Figure 8 shows that a majority of the features used in this work have substantial importance in the random forest classifier for discerning at least one science class. Close inspection of this figure illuminates the usefulness of certain features for distinguishing specific science classes. As expected, the amplitude and frequency of the first harmonic, along with the features related to the spread and skew of the flux measurements, have the highest level of importance. The flux amplitude is particularly important for classifying Mira stars, Cepheids, and RR Lyrae, which are distinguished by their large amplitudes. The frequency of the first harmonic has high importance for most pulsating stars, likely because these classes have similar amplitudes but different frequencies. The QSO variability feature is important for
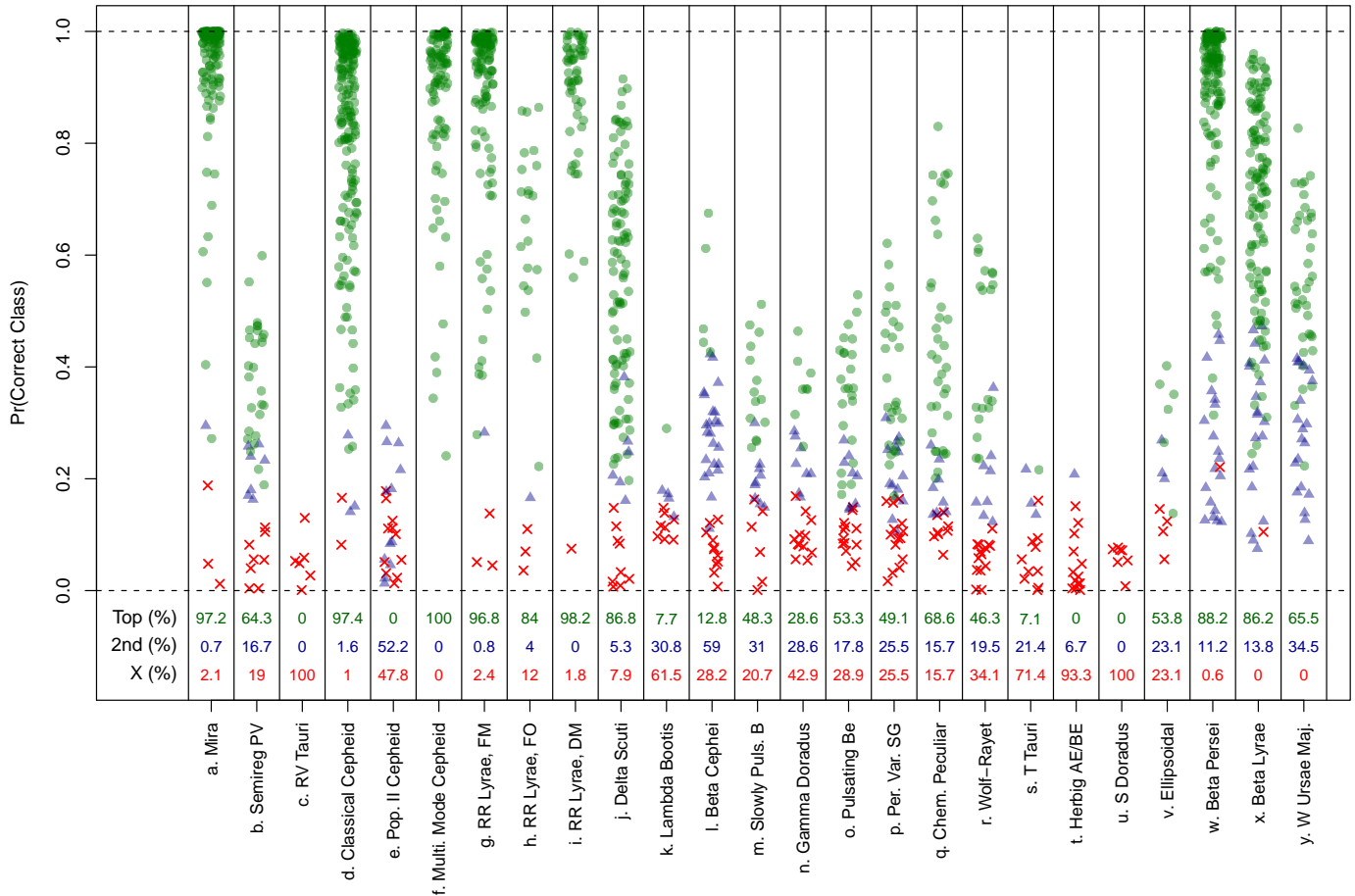
FIG. 6.— Cross-validated random forest probability estimate of the correct class for each variable star, plotted by class. Green circles indicate that the classifier's top choice for that object was correct, blue triangles indicate that the second choice was correct, and red x's indicated that neither of the top two were correct. As a general trend, we find that the classifier performs better for large classes.

identifying eruptive sources, such as Periodically Variable Super Giants and Chemically Peculiar stars, because these stars generally have small values of the QSO feature compared to other variable star classes.

In addition, there are several features that have very low importance for distinguishing any of the science classes. These features include the relative phase offsets for each of the harmonics, the amplitudes of the higher-order harmonics, and non-periodic features such as `beyond1std`, `max_slope`, and `pair_slope_trend`. We rerun the random forest classifier excluding the 14 features with the smallest feature importance (the excluded features are 9 relative phase offsets, `beyond1std`, `max_slope`, `pair_slope_trend`, and the 65th and 80th middle flux percentiles. Results show a cross-validated error rate of 22.8% and a catastrophic error rate of 8.2% (averaged over 10 repetitions of the random forest), which is consistent with the error rates of the random forest trained on all 53 features, showing the insensitivity of the random forest classifier to inclusion of features that carry little or no classification information.

4.8. Classification of high-amplitude (>0.1 mag) sources

High-amplitude variable stars constitute many of the central scientific impetuses of current and future surveys. In particular, finding and classifying pulsational variables with known period-luminosity relationships (Mira, Cepheids and RR Lyrae) is a major thrust of the Large Synoptic Survey Telescope (Walkowicz et al. 2009; LSST Science Collaborations et al. 2009). Moreover, light curves from low-amplitude sources generally have a lower signal-to-noise ratio, making it more difficult to estimate their light-curve derived features and hence more difficult to obtain accurate classifications. Indeed, several of the classes in which we frequently make errors are populated by low-amplitude sources.

Here we classify only those light curves with amplitudes greater than 0.1 mag, removing low-amplitude classes from the sample. This results in the removal of 383 sources, or 25% of the data. After excluding these sources, we are left with a handful of classes with less than 7 sources. Due to the difficulty in training (and cross-validating) a classifier for classes with such small amount of data, we ignore those classes, resulting in the exclusion of 19 more sources, bringing the total to 408 excluded sources, or 26% of the entire data set. We are left with 1134 sources in 16 science classes.

On this subset of data, our random forest classifier achieves a cross-validated misclassification rate of 13.7%, a substantial improvement from the 22.8% misclassification rate from the best classifier on the entire data set. The
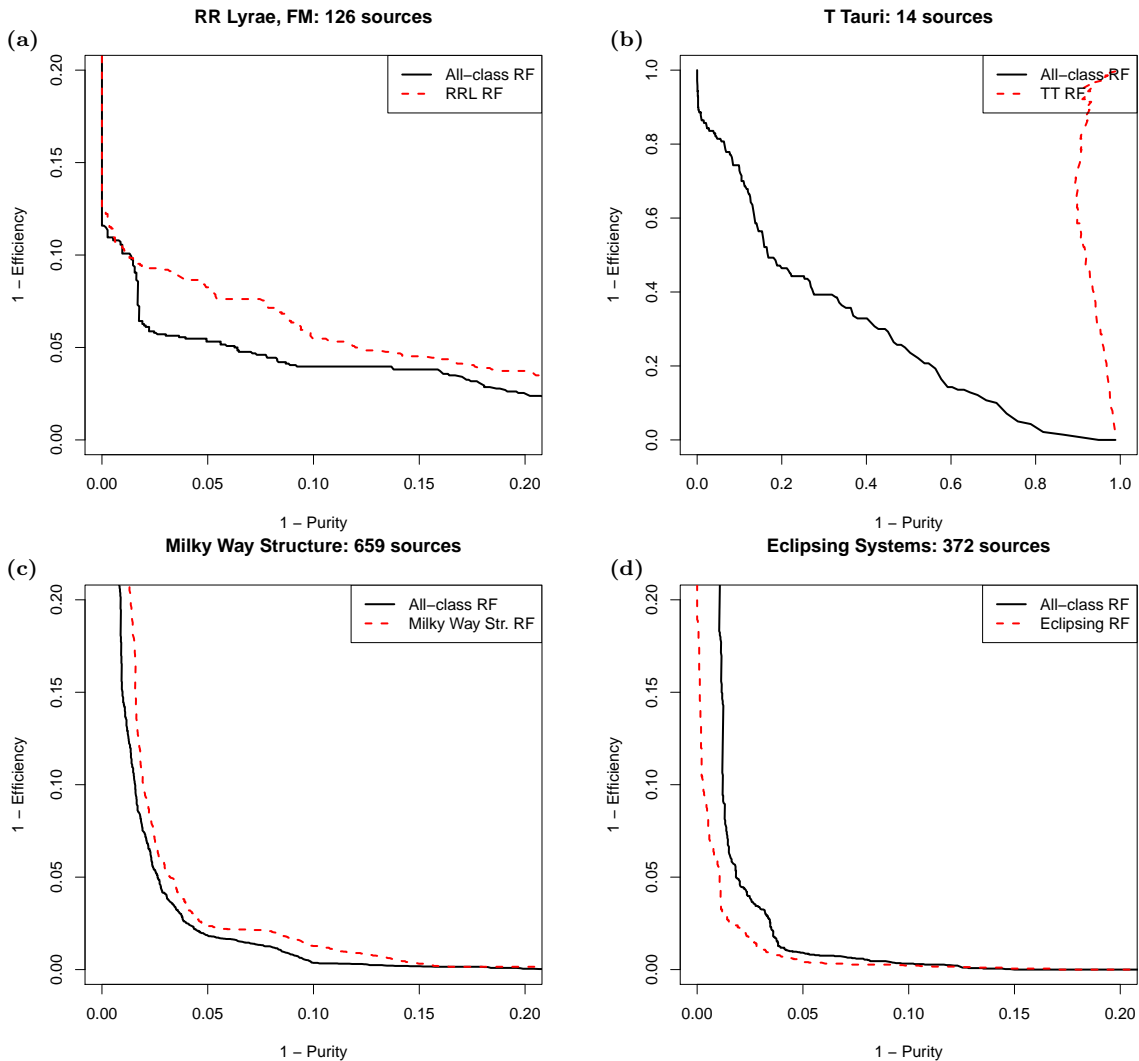
Fig. 7.— Cross-validated ROC curves, averaged over 10 cross validation trials, for four different science classes: (a) RR Lyrae, FM, (b) T Tauri, (c) Milky Way Structure, which includes all Mira, RR Lyrae, and Cepheid stars, and (d) Eclipsing Systems, which includes all Beta Persei, Beta Lyrae, and W Ursae Major stars. Plotted is 1-Efficiency versus 1-Purity as a function of the class threshold. The 25-class random forest ROC curve (solid black line) dominates the ROC curve of a one-versus-all random forest (dashed red line) for each science class except Eclipsing Systems. For T Tauri, the all-class random forest is vastly superior to the T Tauri-specific classifier.

catastrophic misclassification rate is only 3.5%, compared to 8.0% for the entire data set. In figure 9 the confusion matrix for the classifier is plotted. The most prevalent error is misclassifying Pulsating Be and T Tauri stars as semi-regular pulsating variables. On average 8 of the 9 Pulsating Be stars and 4 of the 12 T Tauri stars are misclassified as semi-regular pulsating variables.

4.9. OGLE versus Hipparcos

Data from the sources that we classify in this section come from either the OGLE and Hipparcos surveys. Specifically, there are 523 sources from five science classes whose data are from OGLE, while the data from the remaining 858 sources are from Hipparcos. Our classifiers tend to perform much better for the OGLE data than for the Hipparcos sources: for the random forest classifier we obtain a 11.3% error rate for OGLE data and 27.9% error rate for Hipparcos.

It is unclear whether the better performance for OGLE data is due to the relative ease at classifying the five science classes with OGLE data or because of differences in the survey specifications. The sampling rate of the OGLE survey is three times higher than that of Hipparcos. The average number of observations per OGLE source is 329, compared to 103 for Hipparcos, even though the average time baselines for the surveys are each near 1100 days. OGLE observations have on average twice the flux as Hipparcos observations, but the flux measurement errors of OGLE light curves tend to be higher, making their respective signal-to-noise ratios similar (OGLE flux measurements have on average a SNR 1.25 times higher than Hipparcos SNRs).

To test whether the observed gains in accuracy between OGLE and Hipparcos sources is due to differences in the surveys or differences in the science classes observed by each survey, we run the following experiment: For each OGLE light curve, we thin the flux measurements down to one-third of the original observations to mimic Hipparcos conditions
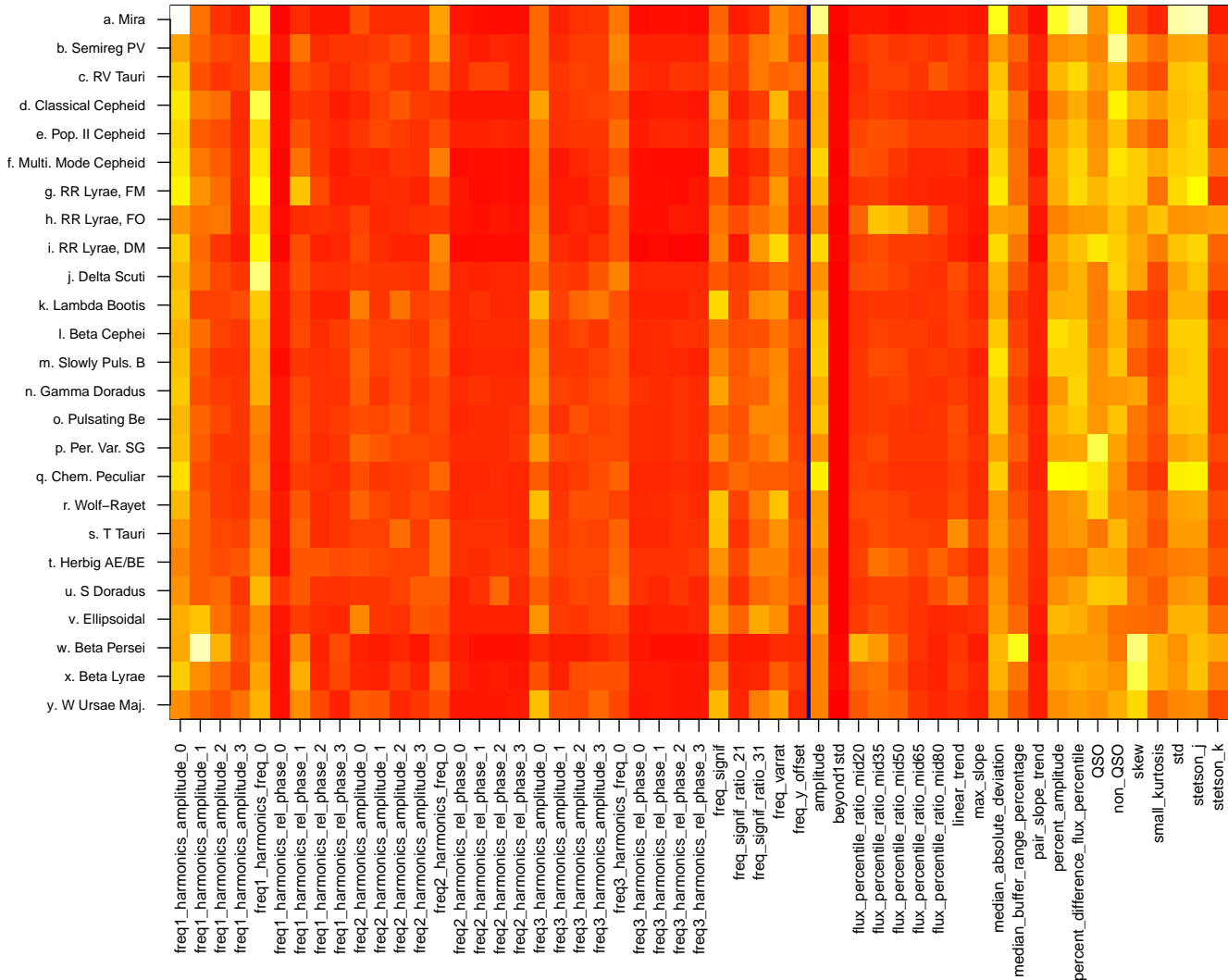
FIG. 8.— Pairwise random forest feature importance. Intensity is the square root of the proportion of instances of each class classified correctly because of that feature (compared to a replacement random permutation of that feature). Features are split into periodic (left) and non-periodic (right) features. The periodic features related to the first frequency are the most important, with higher-order frequencies and harmonics having smaller importance. The non-periodic features related to spread and skew have high importance in the classifier, as do the QSO-variability features.

and re-run the feature extraction pipeline and classifier using the thinned light curves. Note that we do not add noise to the OGLE data because of the relative-similarity in average SNR between the surveys; the dominant difference between data of the two surveys is the sampling rate. Results of the experiment are that the error rate for OGLE data increases to 13.0%, an increase of only 1.7% representing 9 more misclassified OGLE sources. This value remains much lower than the Hipparcos error rate, showing that the better classifier performance for OGLE data is primarily driven by the ease of distinguishing those science classes.

5. CONCLUSIONS AND FUTURE WORK

We have presented a thorough study of automated variable star classification from sparse and noisy single-band light curves. In the 25-class problem considered by Debosscher et al. (2007), which includes all of the most important variable star science classes, we obtain a 24% improvement over their best classifier in terms of misclassification error rate. We attribute this improvement to all of the following advances:

- **Better periodic feature estimation.** Our Lomb-Scargle period-fitting code is both fast and accurate. With the same random forest classifier, the average error rate using our periodic feature estimates is 23.8%, compared to an error rate of 26.7% using only Debosscher's period feature estimates, representing an improvement of 11%.

- **Use of predictive non-periodic features.** Simple summary statistics and more sophisticated model parameters give a significant improvement. Using both our periodic and non-periodic features, the random forest error rate is 22.8%, a 4% improvement over using only our periodic features.
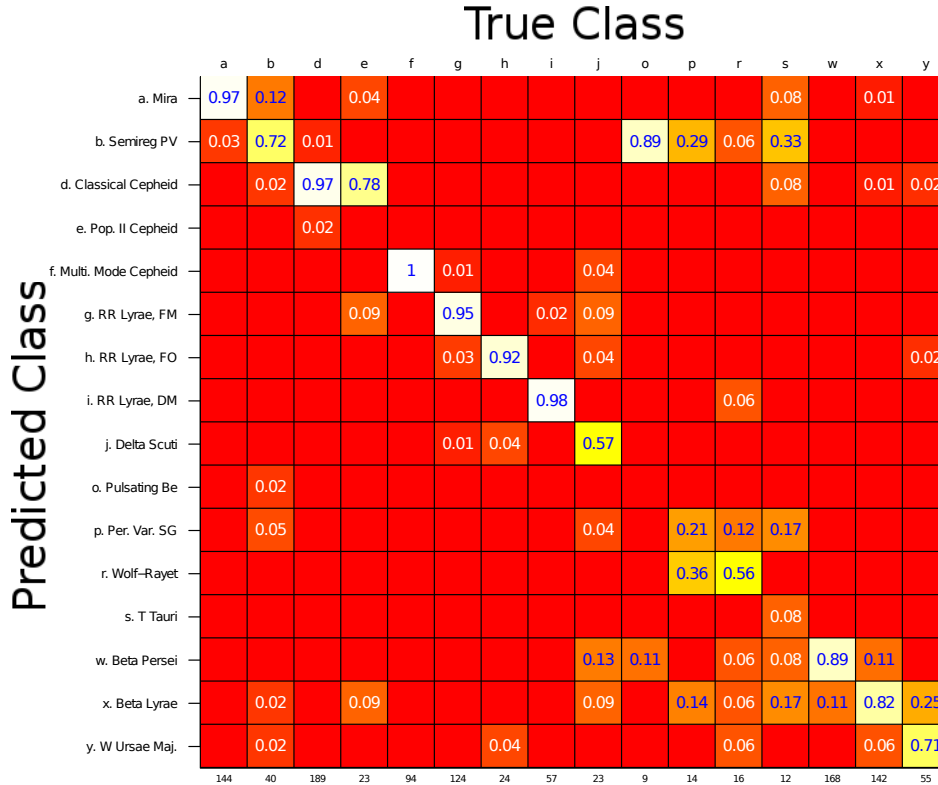
FIG. 9.— Cross-validated confusion matrix for a random forest classifier applied only to the OGLE+Hipparcos sources with amplitude greater than 0.1 magnitude. The overall error rate for this subset of data is 13.7%, with catastrophic misclassification rate of 3.5%.

- **More accurate classification methods.** All of the methods considered in this paper, save the single-tree models, achieve a statistically-significant improvement over Debosscher's best classifier. Our random forest classifier, applied to the exact features used by that paper, achieves an 11% improvement over their best error rate, 30%.

Another contribution is our discussion of model validation through estimation of the expected prediction error on new data by cross-validation. We presented cross-validation as a statistically-rigorous way to both tune a classifier and select between competing methods. Indeed, all of the numbers quoted in this paper are 10-fold cross-validation estimates.

We have shown the adeptness of tree-based classifiers in the problem of variable star classification. We demonstrated the superiority of the random forest classifier in terms of error rates, speed, and immunity to features with little useful classification information. We outlined how to calculate the optimal probability threshold to obtain pure and complete samples of specified sub-classes, and showed that the multi-class random forest is often superior to the one-versus-all random forest in this problem. We advocate the continued use of this method for other classification problems in astronomy.

Furthermore, we described how the random forest classifier can be used to estimate the importance of each feature by computing the expected classification gains versus replacing that feature with random noise. In the variable star classification problem, it was found that several non-periodic features have high importance. A classifier built only on the non-periodic features still performs quite well, attaining 27.6% error rate.

Finally, this paper is the first to use the known variable-star taxonomy both to train a classifier and evaluate its result. We introduced two different classification methods to incorporate a hierarchical taxonomy: HSC, which builds a different classifier in each non-terminal node of the taxonomy, and HMC, which fits a single classifier, penalizing errors at smaller depths in the taxonomy more heavily. We demonstrated that both of these methods perform well, in terms of classification rate and catastrophic error rate. The class taxonomy was also used to construct the notion of catastrophic error rate, which considers as catastrophic any error made at the top level of the hierarchy.

Several open questions remain with regard to the automated classification of astronomical time series. Many of these questions will be addressed by us in future publications, where we will expand on the methodology presented here and attempt to classify data from other surveys, such as the All Sky Automated Survey (ASAS), SDSS Stripe 82, and the Wide Angle Search for Planets (WASP). Some of the questions that we will address are:

- If we train a classifier on a set of objects from one (or multiple) survey(s), will that classifier be appropriate to predict the classes of objects from the new survey? This question is of great importance because presumably a

set of known (labeled) variable stars will be compiled from previous surveys to train a classifier for use on a new survey.

- What features are robust across a wide range of different surveys, each with different cadences? If some sets of features are robust to survey design and cadence, those should be used in lieu of survey-dependent features in a classifier. In this paper, we have excluded any feature that was blatantly survey-dependent (such as any that used mean flux), but this does not guarantee that some features will not have survey dependence.

- How does mis-labelled training data affect the classifier accuracy? Can mis-labelled data be effectively detected and cleaned from the classification set?

- How can a classifier be trained to efficiently identify outliers/new types of variables? Future surveys will unquestionably discover new science classes that do not fit under any of the training classes. Recent methodology has been developed in the statistics literature for outlier discovery in random forest classifiers, and we plan to adapt this for variable star classification.

- How are the error rates of a classifier affected by computational limitations (where, perhaps some CPU-intensive or external server-dependent features are not used)? In automated classification of astronomical sources, there is often a time sensitivity for follow-up observations. Presumably there are more useful features for classification than the ones that we employed in this paper, but they may be expensive to compute or retrieve for each observation. This trade-off between error rate and computation time must be explored.

Finally, as a longer-term goal, we are striving to develop methodology that can be used on a LSST-caliber survey. This means that our methods must be fast enough to compute features and class probabilities for thousands of objects per night, work well at an LSST cadence, be applicable to multi-band light curves, and perform classification for all types of astronomical objects, including transients, variable stars, and QSOs. Our task, looking forward, is to address each of these problems and develop methodology for fast and accurate classification for LSST.

APPENDIX

A. FEATURES ESTIMATED FROM LIGHT CURVES

A description of the 32 periodic features computed using the methodology in §2.1 is in table 4. In addition to these 32 periodic features, we calculate 20 non-periodic features for every light curve (§2.2). These features are compiled in table 5. These consist primarily of simple statistics that can be calculated in the limit of few data points and also when no period is known in order to characterize the flux variation distribution. Where possible, we give the name of the Python function that calculates the feature (e.g., skewness is from `scipy.stats.skew()` in the Python SciPy module).

We begin with basic moment calculations using the observed photometric magnitude *mag* vector for each source:

- `skew`: skewness of the magnitudes: scipy.stats.skew();

- `small_kurtosis`: small sample kurtosis of the magnitudes[11];

- `std`: standard deviation of the magnitudes: Numpy std();

- `beyond1std`: the fraction (≤ 1) of photometric magnitudes that lie above or below one std() from the weighted (by photometric errors) mean;

- `stetson_j`: Stetson (1996) variability index, a robust standard deviation;

- `stetson_k`: Stetson (1996) robust kurtosis measure.

We also calculate the following basic quantities using the magnitudes:

- `max_slope`: examining successive (time-sorted) magnitudes, the maximal first difference (value of delta magnitude over delta time);

- `amplitude`: difference between the maximum and minimum magnitudes;

[11] see `http://www.xycoon.com/peakedness_small_sample_test_1.htm`

- `median_absolute_deviation`: $\mathrm{median}(|mag - \mathrm{median}(mag)|)$;

- `median_buffer_range_percentage`: fraction (≤ 1) of photometric points within amplitude/10 of the median magnitude

- `pair_slope_trend`: considering the last 30 (time-sorted) measurements of source magnitude, the fraction of increasing first differences minus the fraction of decreasing first differences.

We also characterize the sorted flux $F = 10^{-0.4mag}$ distribution using percentiles, following Eyer (2006). If $F_{5,95}$ is the difference between 95% and 5% flux values, we calculate:

- `flux_percentile_ratio_mid20`: ratio $F_{40,60}/F_{5,95}$;

- `flux_percentile_ratio_mid35`: ratio $F_{32.5,67.5}/F_{5,95}$;

- `flux_percentile_ratio_mid50`: ratio $F_{25,75}/F_{5,95}$;

- `flux_percentile_ratio_mid65`: ratio $F_{17.5,82.5}/F_{5,95}$;

- `flux_percentile_ratio_mid80`: ratio $F_{10,90}/F_{5,95}$;

- `percent_amplitude`:the largest absolute departure from the median flux, divided by the median flux;

- `percent_difference_flux_percentile`:ratio of $F_{5,95}$ over the median flux.

Finally, useful for stochastically varying sources, we calculate the quasar similarity metrics from Butler & Bloom (2010):

- `QSO`: quality of fit $\chi^2_{\mathrm{QSO}}/\nu$ for a quasar-like source, assuming $mag = 19$;

- `non_QSO`: quality of fit for a non-quasar-like source (related to NULL value of QSO).

B. DOUBLY-LABELED STARS

As discussed in §4.1, there are 25 sources with more than one class label. Five of these objects are labeled as both S Doradus and periodically-variable super giants. We assign these to the S Doradus class because S Doradus is a subclass of periodically-variable super giants. Two other sources, V* BF Ori and HD 97048 were verified to be Herbig AE/BE type stars by Grinin et al. (2010) and Doering et al. (2007), respectively. RY Lep is listed incorrectly in Simbad as an Agol-type eclipsing system (its original 50-year old classification) and as RR Lyrae/Delta Scuti. Derekas et al. (2009) clearly establish this source as a high-ampltiude δ-Scuti in a binary system. Likewise, HIP 99252 is a δ-Scuti star (Rodríguez et al. 2000) and not also an RR Lyrae. HIP 30326 (=V Mon) is a Mira variable and not also part of the RV Tauri class (Whitelock et al. 2008). HD 210111 (listed also as delta Scuti) is a λ Bootis star (Paunzen & Reegen 2008). HD 165763 is a WR star that is not periodic to a high-degree of confidence (Moffat et al. 2008). Likewise, WR40 is not periodic as it was once believed (Marchenko et al. 1994). We found no reference to the periodic nature of the WR star HD 156385. The remaining 11 sources were of ambiguous class or truly deserved of two classes, and were excluded from the training and testing sample. These stars are listed in table 6, and briefly mentioned below:

- *HD 136488 = HIP 75377*: This is a WR with a measured periodicity in Hipparcos data (Koen & Eyer 2002).

- *HD 94910 = AG Car*: This is a WR is thought to be a "hot, quiescent state LBV" (Clark et al. 2010).

- *HD 50896 = EZ CMa = WR 6*: Listed as both a WR and periodic variable super giant, this is a prototype WR has a known periodic variability possibly due to a binary companion (Flores et al. 2007).

- *HD 37151*: Slowly pulsating B-stars (SPBs) occur in the same instability strip of the H-R diagram as chemically peculiar B stars (with variability associated with rotation and magnetic fields). The classification of this star is particularly ambiguous (see Briquet et al. 2007 and references therein).

- *HD 35715* Is a cataloged Beta Cepheid but is also an ellipsoidal variable (Stankov & Handler 2005). Pulsation was not detected photometrically but in line profiles.

- *HIP34042 (Z CMa A)* Is a binary system consisting of a Herbig component (A) and an FU Orionis star (B) in a close orbit. Determining the photometric contributions of the two components separately is problematic because of strong variability and the small angular separation (Millan-Gabet & Monnier 2002).

- *TV Lyn, UY Cam, V1719 Cyg (HD 200925) & V753 Cen* Ambiguous classification (within the literature) of RR Lyrae or Delta Scuti type stars.

TABLE 4
Periodic features extracted from light curves using generalized Lomb-Scargle

Feature	Description[a]
`freq1_harmonics_amplitude_0`	$A_{1,1}$[b]
`freq1_harmonics_amplitude_1`	$A_{1,2}$
`freq1_harmonics_amplitude_2`	$A_{1,3}$
`freq1_harmonics_amplitude_3`	$A_{1,4}$
`freq1_harmonics_freq_0`	f_1[c]
`freq1_harmonics_rel_phase_0`	$PH_{1,1}$[d]
`freq1_harmonics_rel_phase_1`	$PH_{1,2}$
`freq1_harmonics_rel_phase_2`	$PH_{1,3}$
`freq1_harmonics_rel_phase_3`	$PH_{1,4}$
`freq2_harmonics_amplitude_0`	$A_{2,1}$
`freq2_harmonics_amplitude_1`	$A_{2,2}$
`freq2_harmonics_amplitude_2`	$A_{2,3}$
`freq2_harmonics_amplitude_3`	$A_{2,4}$
`freq2_harmonics_freq_0`	f_2
`freq2_harmonics_rel_phase_0`	$PH_{2,1}$
`freq2_harmonics_rel_phase_1`	$PH_{2,2}$
`freq2_harmonics_rel_phase_2`	$PH_{2,3}$
`freq2_harmonics_rel_phase_3`	$PH_{2,4}$
`freq3_harmonics_amplitude_0`	$A_{3,1}$
`freq3_harmonics_amplitude_1`	$A_{3,2}$
`freq3_harmonics_amplitude_2`	$A_{3,3}$
`freq3_harmonics_amplitude_3`	$A_{3,4}$
`freq3_harmonics_freq_0`	f_3
`freq3_harmonics_rel_phase_0`	$PH_{3,1}$
`freq3_harmonics_rel_phase_1`	$PH_{3,2}$
`freq3_harmonics_rel_phase_2`	$PH_{3,3}$
`freq3_harmonics_rel_phase_3`	$PH_{3,4}$
`freq_signif`	Significance of f_1 vs. null hypothesis of white noise with no periodic variation, computed using a Student's-T distribution
`freq_signif_ratio_21`	Ratio of significance of f_2 vs. null to f_1 vs. null
`freq_signif_ratio_31`	Ratio of significance of f_3 vs. null to f_1 vs. null
`freq_varrat`	Ratio of the variance after, to the variance before subtraction of the fit with f_1 and its 4 harmonics
`freq_y_offset`	c

[a] Notation from discussion of Lomb-Scargle periodic feature extraction in §2.1 is used.
[b] All amplitudes are in units of magnitude.
[c] All frequencies are in units of cycles/day.
[d] All relative phases are unitless ratios.

TABLE 5
Non-periodic features extracted from light curves

Feature	Description
`amplitude`	Half the difference between the maximum and the minimum magnitude
`beyond1std`	Percentage of points beyond one st. dev. from the weighted mean
`flux_percentile_ratio_mid20`	Ratio of flux percentiles (60th - 40th) over (95th - 5th)
`flux_percentile_ratio_mid35`	Ratio of flux percentiles (67.5th - 32.5th) over (95th - 5th)
`flux_percentile_ratio_mid50`	Ratio of flux percentiles (75th - 25th) over (95th - 5th)
`flux_percentile_ratio_mid65`	Ratio of flux percentiles (82.5th - 17.5th) over (95th - 5th)
`flux_percentile_ratio_mid80`	Ratio of flux percentiles (90th - 10th) over (95th - 5th)
`linear_trend`	Slope of a linear fit to the light curve fluxes
`max_slope`	Maximum absolute flux slope between two consecutive observations
`median_absolute_deviation`	Median discrepancy of the fluxes from the median flux
`median_buffer_range_percentage`	Percentage of fluxes within 20% of the amplitude from the median
`pair_slope_trend`	Percentage of all pairs of consecutive flux measurements that have positive slope
`percent_amplitude`	Largest percentage difference between either the max or min magnitude and the median
`percent_difference_flux_percentile`	Diff. between the 2nd & 98th flux percentiles, converted to magnitude[a]
`QSO`	Quasar variability metric in Butler & Bloom (2010)
`non_QSO`	Non-quasar variability metric in Butler & Bloom (2010)
`skew`	Skew of the fluxes
`small_kurtosis`	Kurtosis of the fluxes, reliable down to a small number of epochs
`std`	Standard deviation of the fluxes
`stetson_j`	Welch-Stetson variability index J[b]
`stetson_k`	Welch-Stetson variability index K[b]

[a] Eyer (2005)
[b] Stetson (1996)

TABLE 6
Doubly-labelled sources excluded from the sample for both training and testing purposes.

RA	Dec	ID	Class 1 [a]	Class 2 [a]	RF best class [b]	RF 2nd best class [c]
05 26 50.2284	+03 05 44.428	HD 35715	l. Beta Cephei	v. Ellipsoidal	m. Slowly Puls. B (0.214)	v. Ellipsoidal (0.164)
05 36 06.2333	−07 23 47.320	HD 37151	q. Chem. Peculiar	m. Slowly Puls. B	p. Per. Var. SG (0.211)	n. Gamma Doradus (0.155)
06 54 13.0441	−23 55 42.011	HD 50896	r. Wolf-Rayet	p. Per. Var. SG	v. Ellipsoidal (0.181)	o. Pulsating Be (0.145)
07 03 43.1619	−11 33 06.209	HIP 34042	t. Herbig AE/BE	s. T Tauri	b. Semireg PV (0.287)	d. Classical Cepheid (0.114)
07 33 31.7288	+47 48 09.823	TV Lyn	j. Delta Scuti	h. RR Lyrae, FO	h. RR Lyrae, FO (0.686)	g. RR Lyrae, FM (0.12)
07 58 58.8801	+72 47 15.411	UY Cam	j. Delta Scuti	h. RR Lyrae, FO	h. RR Lyrae, FO (0.236)	j. Delta Scuti (0.222)
10 56 11.5763	−60 27 12.815	HD 94910	r. Wolf-Rayet	u. S Doradus	b. Semireg PV (0.258)	a. Mira (0.243)
11 51 15.3088	−55 48 15.795	V753 Cen	j. Delta Scuti	h. RR Lyrae, FO	h. RR Lyrae, FO (0.469)	j. Delta Scuti (0.151)
12 04 47.2738	−27 40 43.295	IK Hya	e. Pop. II Cepheid	g. RR Lyrae, FM	g. RR Lyrae, FM (0.456)	y. W Ursae Maj. (0.100)
15 24 11.3087	−62 40 37.567	HD 136488	p. Per. Var. SG	r. Wolf-Rayet	r. Wolf-Rayet (0.161)	p. Per. Var. SG (0.147)
21 04 32.9211	+50 47 03.276	V1719 Cyg	j. Delta Scuti	h. RR Lyrae, FO	j. Delta Scuti (0.315)	y. W Ursae Maj. (0.226)

[a] Classes determined by Debosscher et al. (2007).
[b] Most likely class determined by a random forest classifier. Posterior probability in parentheses.
[c] Second-best candidate class determined by a random forest classifier. Posterior probability in parentheses.

- *IK Hya* Is a short-period Pop. II Cepheid, making it likely a BL Herculis type star.

We trained a random forest classifier on the features of only the single-labeled stars, and then predicted the class probabilities of each label for the doubly-labeled stars. This experiment shows that for 7 of the 11 sources, our classifier predicts one of the two classes that the star was originally labeled as. Note that recently, several methods have been developed to classify data with multiple labels (multi-label classification, see Tsoumakas & Katakis 2007), but for the purposes of this work we choose to only perform single-label classification, and remove these data from our sample to avoid biases from inaccurate training labels.

REFERENCES

Bailey, S., Aragon, C., Romano, R., Thomas, R. C., Weaver, B. A., & Wong, D. 2007, ApJ, 665, 1246
Ball, N. M., Brunner, R. J., Myers, A. D., & Tcheng, D. 2006, ApJ, 650, 497
Barning, F. J. M. 1963, Bull. Astron. Inst. Netherlands, 17, 22
Blockeel, H., Schietgat, L., Struyf, J., Džeroski, S., & Clare, A. 2006, Knowledge Discovery in Databases: PKDD 2006, 18
Blomme, J., et al. 2010, ApJ, 713, L204
Breiman, L. 1996, Machine learning, 24, 123
—. 2001, Machine learning, 45, 5
Breiman, L., Friedman, J., Olshen, R., & Stone, C. 1984, Wadsworth Inc, 67
Brett, D. R., West, R. G., & Wheatley, P. J. 2004, MNRAS, 353, 369
Briquet, M., Hubrig, S., De Cat, P., Aerts, C., North, P., & Schöller, M. 2007, A&A, 466, 269
Burman, P. 1989, Biometrika, 76, 503
Butler, N. R., & Bloom, J. S. 2010, arXiv e-print 1008.3143
Cesa-Bianchi, N., Gentile, C., & Zaniboni, L. 2006, The Journal of Machine Learning Research, 7, 31
Cheeseman, P., & Stutz, J. 1996, Advances in knowledge discovery and data mining, 180
Clark, J. S., Ritchie, B. W., & Negueruela, I. 2010, A&A, 514, A87
Covey, K. R., et al. 2007, AJ, 134, 2398
Debosscher, J., Sarro, L. M., Aerts, C., Cuypers, J., Vandenbussche, B., Garrido, R., & Solano, E. 2007, A&A, 475, 1159
Derekas, A., et al. 2009, MNRAS, 394, 995
Doering, R. L., Meixner, M., Holfeltz, S. T., Krist, J. E., Ardila, D. R., Kamp, I., Clampin, M. C., & Lubow, S. H. 2007, AJ, 133, 2122
Eads, D. R., Williams, S. J., Theiler, J., Porter, R., Harvey, N. R., Perkins, S. J., Brumby, S. P., & David, N. A. 2004, in Society of Photo-Optical Instrumentation Engineers (SPIE) Conference Series, ed. B. Bosacchi, D. B. Fogel, and J. C. Bezdek, Vol. 5200, 79–90
Eyer, L. 2005, in ESA Special Publication, Vol. 576, The Three-Dimensional Universe with Gaia, ed. C. Turon, K. S. O'Flaherty, and M. A. C. Perryman, 513
Eyer, L. 2006, in Astronomical Society of the Pacific Conference Series, Vol. 349, Astrophysics of Variable Stars, ed. C. Aerts and C. Sterken, 15

Eyer, L., & Blake, C. 2005, MNRAS, 358, 30
Eyer, L., & Mowlavi, N. 2008, Journal of Physics Conference Series, 118, 012010
Eyer, L., et al. 2008, in American Institute of Physics Conference Series, Vol. 1082, American Institute of Physics Conference Series, ed. C. A. L. Bailer-Jones, 257–262
Flores, A., Koenigsberger, G., Cardona, O., & de la Cruz, L. 2007, AJ, 133, 2859
Freund, Y., & Schapire, R. 1996, in International Conference on Machine Learning, 148–156
Friedman, J. 1996, technical report, Department of Statistics, Stanford University
Friedman, J. H. 2001, The Annals of Statistics, 29, pp. 1189
Gregory, P. C. 2005, Bayesian Logical Data Analysis for the Physical Sciences: A Comparative Approach with 'Mathematica' Support (Cambridge University Press)
Grinin, V. P., Rostopchina, A. N., Barsunova, O. Y., & Demidova, T. V. 2010, Astrophysics, 53, 367
Hastie, T., & Tibshirani, R. 1998, Annals of Statistics, 26, 451
Hastie, T., Tibshirani, R., & Friedman, J. 2009, The Elements of Statistical Learning: Data Mining, Inference, and Prediction., 2nd edn. (Springer, New York)
Horne, J. H., & Baliunas, S. L. 1986, ApJ, 302, 757
Ivezić, Ž., et al. 2007, AJ, 134, 973
Kessler, R., et al. 2010, PASP, 122, 1415
Knerr, S., et al. 1990, Optimization Methods and Software, 1, 23
Koen, C., & Eyer, L. 2002, MNRAS, 331, 45
Lomb, N. R. 1976, Ap&SS, 39, 447
LSST Science Collaborations et al. 2009, arXiv e-print 0912.0201
Mahabal, A., et al. 2008, Astronomische Nachrichten, 329, 288
Marchenko, S. V., Antokhin, I. I., Bertrand, J., Lamontagne, R., Moffat, A. F. J., Piceno, A., & Matthews, J. M. 1994, AJ, 108, 678
Millan-Gabet, R., & Monnier, J. D. 2002, ApJ, 580, L167
Moffat, A. F. J., et al. 2008, ApJ, 679, L45
O'Keefe, P. J., Gowanlock, M. G., McConnell, S. M., & Patton, D. 2009, in Astronomical Society of the Pacific Conference Series, Vol. 411, Astronomical Society of the Pacific Conference Series, ed. D. A. Bohlender, D. Durand, and P. Dowler, 318
Paunzen, E., & Reegen, P. 2008, Communications in Asteroseismology, 153, 49
Perryman, M., et al. 1997, Astronomy and Astrophysics, 323, L49

Press, W., Vetterling, W., Teukolsky, S., & Flannery, B. 2001,
    Numerical recipes in C++: the art of scientific computing
    (Cambridge University Press New York, NY, USA)
Quinlan, J. 1996, in Proceedings of the National Conference on
    Artificial Intelligence, 725–730
Rodríguez, E., López-González, M. J., & López de Coca, P. 2000,
    A&AS, 144, 469
Sarro, L. M., Debosscher, J., López, M., & Aerts, C. 2009, A&A,
    494, 739
Scargle, J. D. 1982, ApJ, 263, 835
Sesar, B., et al. 2007, AJ, 134, 2236
Shin, M., Sekora, M., & Byun, Y. 2009, MNRAS, 400, 1897
Silla, C., & Freitas, A. 2011, Data Mining and Knowledge
    Discovery, 22, 31
Stankov, A., & Handler, G. 2005, ApJS, 158, 193
Stetson, P. B. 1996, PASP, 108, 851
Suchkov, A. A., Hanisch, R. J., & Margon, B. 2005, AJ, 130, 2439
Tsoumakas, G., & Katakis, I. 2007, International Journal of Data
    Warehousing and Mining, 3, 1

Udalski, A., Soszynski, I., Szymanski, M., Kubiak, M.,
    Pietrzynski, G., Wozniak, P., & Zebrun, K. 1999, Acta Astron.,
    49, 1
Vapnik, V. 2000, The Nature of Statistical Learning Theory
    (Springer-Verlag, New York)
Vens, C., Struyf, J., Schietgat, L., Džeroski, S., & Blockeel, H.
    2008, Machine Learning, 73, 185
Walkowicz, L. M., et al. 2009, arXiv e-print 0902.3981
Wasserman, L. 2006, All of nonparametric statistics
    (Springer-Verlag, New York)
Whitelock, P. A., Feast, M. W., & van Leeuwen, F. 2008,
    MNRAS, 386, 313
Willemsen, P. G., & Eyer, L. 2007, arXiv e-print 0712.2898
Woźniak, P. R., Williams, S. J., Vestrand, W. T., & Gupta, V.
    2004, AJ, 128, 2965
Wu, T., Lin, C., & Weng, R. 2004, The Journal of Machine
    Learning Research, 5, 975
Zechmeister, M., & Kürster, M. 2009, A&A, 496, 577